

Review

Recent advances and future prospects of the potential-resolved strategy in ratiometric, multiplex, and multicolor electrochemiluminescence analysis

Shijun Wang^{1#}, Shu Zhu^{1#}, Ziqi Kang^{1#}, Yidan Chen², Xiancheng Liu², Zixin Deng¹, Kun Hu¹, Guixue Wang^{2,3✉}, Yuchan Zhang^{1✉}, Guangchao Zang^{1,3✉}

1. Institute of Life Science, and Laboratory of Tissue and Cell Biology, Lab Teaching & Management Center, Chongqing Medical University, Chongqing, 400016, China.
2. Key Laboratory for Biorheological Science and Technology of Ministry of Education, State and Local Joint Engineering Laboratory for Vascular Implants, Bioengineering College of Chongqing University, Chongqing, 400030, China.
3. Jinfeng Laboratory, Chongqing, 401329, China.

#These authors contributed equally to this work.

✉ Corresponding authors: **Guangchao Zang, PhD**, E-mail: zangguangchao@cqmu.edu.cn, Tel: +86-23-65712090; **Guixue Wang, PhD**, E-mail: wanggx@cqu.edu.cn, Tel: +86-23-65112675; **Yuchan Zhang, PhD**, E-mail: zhangyc@cqmu.edu.cn, Tel: +86-23-65712090.

© The author(s). This is an open access article distributed under the terms of the Creative Commons Attribution License (<https://creativecommons.org/licenses/by/4.0/>). See <http://ivyspring.com/terms> for full terms and conditions.

Received: 2022.04.23; Accepted: 2022.09.09; Published: 2022.09.21

Abstract

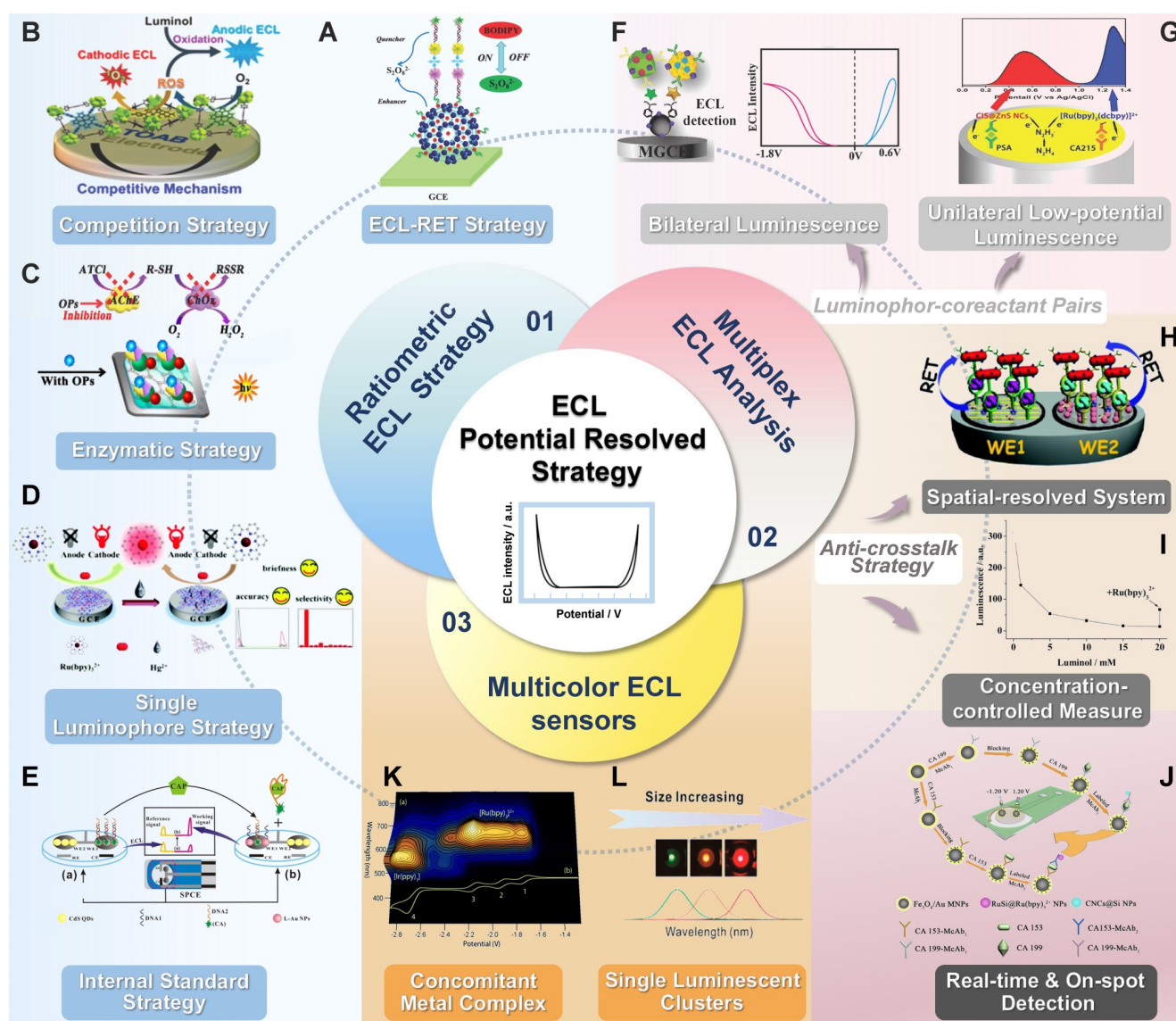
The potential-resolved strategy has gradually demonstrated its distinct values in electrochemiluminescence (ECL) bio-sensing due to its superior characteristics, such as low instrument requirement, short assay time, and improved sample throughput, in conjunction with spatial- and spectrum-resolved techniques. It has recently been widely generalized into versatile multiple-signal ECL analytic platforms, especially in ratiometric and multiplex ECL sensors, in accordance with some specific principles. Furthermore, luminophore pairs with potential- and wavelength-resolved properties have been utilized to visualize biosensors that display multiple colors depending on analyte concentration. However, only a few comprehensive reports on the principles, construction, and application of various ECL sensors in potential-resolved schemes have been published. This review aims to recount the potential-resolved strategy applying to (a) ratiometric ECL sensors, (b) multiplex ECL sensors, and (c) multicolor ECL sensors and to discuss the distinctions and connections among the application principles of these strategies. Finally, the future prospects of ECL-based potential-resolved analysis are explored.

Key words: electrochemiluminescence, potential-resolved strategy, ratiometric electrochemiluminescence sensors, multiplex electrochemiluminescence sensors, multicolor electrochemiluminescence sensors

Introduction

Electrochemiluminescence (ECL), which combines chemiluminescence and electrochemistry, is the optical emission from the excited luminophores that are produced at the electrode surface via electrochemical high-energy electron transfer reactions [1,2]. ECL sensors have recently been widely used in biomedical tests, including tests for drug residues, toxic metal ions, tumor biomarkers, DNA, and even circulating tumor cells and exosomes [2-6] because of their high sensitivity, facile controllability, and simple optical equipment requirements [5,7]. However, the majority of the previously reported ECL

analysis systems are built on the basis of a single signal output strategy ("signal-on" or "signal-off" mode). This situation restricts the simultaneous detection of multiple biomarkers or the self-calibration of output signals, thus resulting in decreased efficiency, stability, and accuracy [8]. Therefore, multisignal output strategies, which exploit multidimensional resolvable signal types and multipass signal accesses [9] and therefore allow for the integration and miniaturization of biosensors that detect multiple targets [10,11], will be a future trend in the research on ECL sensors.



Scheme 1. Illustration of the application of potential-resolved strategy in ratiometric ECL sensors based on (A) ECL-RET strategy, adapted with permission from [45], copyright 2020 Elsevier B.V., (B) competition strategy, adapted with permission from [65], copyright 2020 American Chemical Society, (C) enzymatic strategy, adapted with permission from [75], copyright 2017 American Chemical Society, (D) single luminophore strategy, adapted with permission from [84], copyright 2020 Royal Chemical Society, (E) internal standard strategy, adapted with permission from [89], copyright 2016 Elsevier B.V.; multiplex ECL sensors based on (F) bilateral luminescence, adapted with permission from [127], copyright 2020 Elsevier B.V., (G) unilateral low-potential luminescence, adapted with permission from [16], copyright 2021 Elsevier B.V., (H) spatial-resolved system, adapted with permission from [131], copyright 2019 Royal Chemical Society, (I) concentration-controlled measure, adapted with permission from [119], copyright 2014 American Chemical Society, (J) real-time & on-spot detection, adapted with permission from [123], copyright 2013 Elsevier B.V.; and multicolor ECL sensors based on (K) concomitant metal complex, adapted with permission from [182], copyright 2016 Royal Chemical Society, (L) single luminescent clusters, adapted with permission from [205], copyright 2020 American Chemical Society.

The multiple-signal ECL assay accomplishes its principle by using resolvable signal output probes or by using multichannel detection. Signal-resolving schemes are widely used and can be classified into three categories: spatial-resolved [12,13], spectrum-resolved [14,15], and potential-resolved [16,17]. As part of the spatial-resolved technique, segregated sensing arrays on electrode plates are highly sophisticated and exhibit low cross-talk from adjoining sensing zones [18,19]. However, the lack of luminous probe pairs with various emission spectra restricts the deployment of the spectrum-resolved ECL method [20]. Furthermore, the uneven photon

cross-efficiency caused by combining two or more filters to differentiate photons of different wavelengths could reduce the detection sensitivity and accuracy [21,118]. In contrast to the latter two modes, the potential-resolved strategy could achieve multisignal outputs in the same working zone by using only a simple potential scan, thus obviating the need for optical instruments and complex electrode construction, greatly simplifying the operation procedure, and reducing analytical time [22]. Therefore, compared with the other two strategies, the potential-resolved technique appears to be a more viable and attractive strategy for ECL sensing

schemes with multisignal output.

The potential-resolved ECL multisignal strategy is expected to be generalized to versatile sensing platforms, particularly ratiometric ECL sensors and ECL sensors that simultaneously detect multiple markers, for practical biomedical applications. In addition, its use in potential-resolved multicolor ECL (PRMCECL) has grown in popularity in recent years. For this reason, this review provides a comprehensive summary of how the potential-resolved technique is designed and executes its distinctive function with (a) ratiometric ECL sensors, (b) ECL sensors that simultaneously detect multiple markers, and (c) multicolor ECL sensors. Achievements in this area are also discussed. This review also clarifies the distinction and connection among the participation of the three types of ECL sensors in the potential-resolved strategy. Finally, future perspectives for ECL-based potential-resolved analysis are discussed.

Ratiometric ECL Sensors in the Potential-resolved Strategy

The ECL ratiometric approach uses two distinct signal probes to functionalize the electrode substrate and label material and applies the output signal ratio as the concentration indicator. By self-calibrating two luminescent signals, this dual-response detection strategy can suppress the influence of signal interference, such as microenvironmental pollution

[23], from the substrate and the detection system, as well as simplify operation steps [24] and accelerate electron transfer kinetics [25] to improve detection accuracy.

Given the importance of the two ECL output signals with potential-resolvable properties in implementing the ratiometric approach, two rules should be adopted to facilitate ratiometric detection. First, the dual-potential emissions should be composed of two signals that can be distinguished at different excitation potentials [26]. In addition, the same co-reactant of luminophores should be used to minimize mutual electrochemical interference [27].

The sensitivity and repeatability of the sensor are highly influenced by the sensor's construction principles [28]. Many approaches have been used to achieve dual signal output in practice. Among these approaches, the resonance energy transfer (RET) strategy, co-reactant competition strategy, and internal standard strategy are the most prevalent. New ratiometric designs arose as a result of the complexity of chemical compounds and the limited number of accessible luminescent systems. These designs may be characterized as immunological competition, spatial competition, and enzyme-based ratiometric methods. These new methodologies broaden the scope of feasible resolution solutions and provide novel concepts for multisignal output systems.

Table 1. Summary of the partial reports on potential-resolved ratiometric ECL analyses based on the ECL-RET strategy or/and intermediate reagent strategy. Unavailable measurements are represented by "-"

Sensing strategies	Donor	Acceptor	Linear range	LOD	Target	Ref.
RET/intermediate reagent	CdS-CNFS	Luminol-AuNPs	1.0×10^{-16} - 1.0×10^{-15} g/mL	3.3×10^{-14} g/mL	Carcinoembryonic antigen	[57]
	CdS NCs	Luminol-AuNPs	-	5.0×10^{-13} g/mL	Thrombin	[52]
	CdS QDs	Au@luminol	1.0×10^{-5} - 1.0×10^{-2} M	2.8×10^{-6} M	Mg ²⁺	[30]
	g-CdTe QDs	TAEA-Ru	1.0×10^{-14} - 1.0×10^{-9} M	2.9×10^{-12} M	DA	[42]
	CdSe/ZnS QDs	Luminol	5.0×10^{-10} - 5.0×10^{-7} g/mL	-	Prostate specific antigen	[34]
	g-C ₃ N ₄ NSs	Ag-PAMAM-luminol	2.0×10^2 - 9.0×10^3 cells/mL	1.5×10^2 cells/mL	HL-60 cancer cells	[5]
	CdSe/ZnS	Au-Luminol NPs	5.0×10^{-16} - 5.0×10^{-13} M	1.2×10^{-16} M	Target DNA	[46]
	CdTe/CdS/ZnS QDs	DNA2/H/Au	5.0×10^{-12} - 1.0×10^{-8} M	1.2×10^{-13} M	AFB1	[39]
	GQDs	Luminol-AuNPs	1.0×10^{-2} - 1.0×10 U/mL	5.0×10^{-13} U/mL	Protein kinase A	[24]
	CdS NCs	Luminol	5.0×10^{-16} - 1.0×10^{-14} M	2.4×10^{-16} M	Duplex-specific nuclease	[51]
RET	O ₂ /S ₂ O ₈ ²⁻	PTC-NH ₂	1.0×10^{-12} - 1.0×10^{-7} M	3.5×10^{-13} M	Pb ²⁺	[58]
	CdS QDs	Luminol	1.0×10^{-11} - 2.0×10^{-6} M	3.0×10^{-12} M	Pb ²⁺	[59]
	MPA-CdS:Eu NCs	Luminol	1.0 - 3.0×10 U/mL	7.0×10^{-2} U/mL	Human methyltransferase	[60]
	CdSe QDs	Luminol	5.0×10^{-6} - 1.0×10^{-4} M	5.0×10^{-6} M	H ₂ O ₂	[38]
	CdTe@CdS QDs	Luminol	1.0×10^{-7} - 5.0×10^{-13} g/mL	4.2×10^{-15} g/mL	Thrombin	[23]
	CdS QDs	Au-Luminol	-	1.3×10^{-13} g/mL	Carcinoembryonic antigen	[47]
	K ₂ S ₂ O ₈	Fluoroboron dipyrrole	1.0×10^{-13} - 8.5×10^{-7} g/mL	4.2×10^{-14} g/mL	Lactoferrin	[45]
	HCNS	CPB	1.0×10^3 - 3.2×10^5 cells/ mL	3.2×10^2 cells/ mL	MCF-7 cells and CD44 receptors	[40]
	g-C ₃ N ₄	PANI/ABEI	1.0×10^{-13} - 4.0×10^{-11} g/mL	2.3×10^{-14} g/mL	CT	[61]
	CdS NCs	Luminol	5.0×10^{-15} - 1.0×10^{-12} M	1.7×10^{-15} M	mp53 oncogene	[36]
Ru-Lu JPs	FAM/Cy5	1.0×10^{-14} - 1.0×10^{-8} M	8.7×10^{-15} / 1.2×10^{-15} M	miRNA-21/miRNA-155	[43]	
SnS ₂ QDs@Eu MOFs	L-Au-Pt NRs	1.0×10^{-11} - 1.0×10^{-7} M	3.2×10^{-13} M	KAN	[44]	

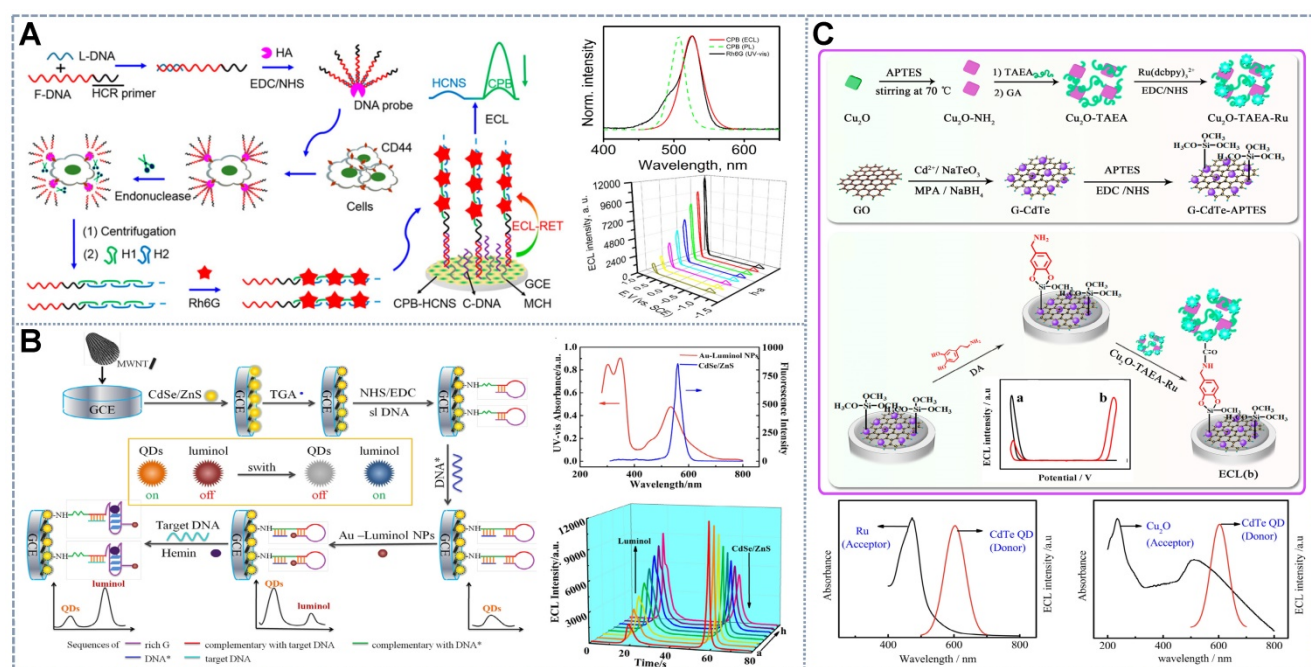


Figure 1. Schematic of the potential resolved ECL-RET biosensors based on (A) the ECL-RET system with luminophores with high color purity and facile band controllability. Adapted with permission from [40], copyright 2020 American Chemical Society; (B) universal enhancer or quencher. Adapted with permission from [51], copyright 2018 Elsevier B.V.; and (C) signal regulation materials. Adapted with permission from [55], copyright 2016 Elsevier B.V.

ECL-RET Strategy

The ECL-RET approach involves the energy transfer between a pair of ECL luminophores or between luminophores and intermediate reagents. It generally results in ECL signal conversion from “off-on” to “on-off”. The emergence of RET requires spectrum overlap between the ECL energy donor and the energy acceptor at an appropriate distance [19]. ECL-RET has attracted considerable attention as a sensitive and controllable ECL signal regulation strategy for the detection of metals [29-31], proteins [32-34], nucleic acids [35-37], small molecules [38,39], and even cells [40,41]. Ideal RET pairs for ratiometric ECL fabrication should present reversible signal changes following the increase in concentration, distinct emission potentials, and minimal interluminophore cross-talk. Since CdS quantum dots (QDs)/Tris-(bipyridine)-Ru (II) ($\text{Ru}(\text{bpy})_3^{2+}$), the first donor and receptor pair, was developed, many novel potential-resolved RET pairs with unique properties have been exploited for ratiometric ECL sensors [42] (Table 1). For example, Han *et al.* [43] developed novel dual-ECL luminescent Janus particles (JPs), which are asymmetric heterostructures comprising Ru (II) complexes and luminol polymers. They enable the simultaneous generation of two strong ECL emissions while eliminating potential signal interference, reducing background interference, and improving ECL intensity. An ultrasensitive dual-quenching Janus ECL-RET strategy using Ru-Lu JPs and dyes

(FAM and cyanine dye (Cy5) as donors-acceptors combined with catalytic hairpin assembly amplification) was proposed for the simultaneous determination of dual-miRNAs. Similarly, Li *et al.* [44] developed a dual-potential ECL platform based on the RET system between SnS_2 QD hybrid Eu metal-organic frameworks (MOFs) as the cathodic emitter and luminol-capped Pt-tipped Au bimetallic nanorods as the anodic luminophor for ultrasensitive KAN detection.

However, some ECL-RET systems cannot realize ideal energy transfer between luminophores [45]. So, some materials that help control ECL emissions, like catalytic (hemin/G-quadruplex DNAzyme [34], horseradish peroxidase (HRP)/AuNRs [36]), carriers (poly(amidoamine) (PAMAM), TiO_2 mesocrystals, helical carbon nanotube (HCNTs) [46]) or quencher (GO [23], Cy5 [39]) are introduced into ratiometric systems. For example, Hao *et al.* [47] introduced Au-luminol and CdS QDs as signal probes in an aptasensor. However, the deficient RET properties of the aptasensor hindered its application in ratiometric systems. Therefore, the quencher fluorophore Cy5 was combined with CdS QDs to perform ECL-RET with luminol and amplify the CdS QD signal. These effects enabled the self-tuning of the two emissions. Similarly, as shown in Figure 1A, Cao *et al.* [40] proposed CsPbBr_3 nanocrystal (CPB), which acted as an ECL emitter with high color purity (with a full-width-at-half-maximum (FWHM) of 12-25 nm) and facile band tunability through halogen exchange.

These characteristics make CPB a perfect ECL donor and facilitate the search for available ECL receptors. Then, the all-inorganic perovskite anodic emitter CPB was *in situ* assembled into hollow graphitic carbon nitride nanospheres (HCNSs) for a matching band-edge arrangement to enhance its ECL performance. The HCNSs also served as the cathodic emitters for ratiometric analysis. Given that the emitter complex lacked signal regulation ability, rhodamine 6G (Rh6G) was introduced into the system. Rh6G can be loaded onto the long DNA duplexes generated through the hybridization chain reaction triggered by the addition of the detector and subsequently dramatically quench the anodic ECL of CPB. Therefore, the signal from CPB indicated the analyte concentration and that from HCNS was used as an internal standard to calibrate the signal. However, the application of RET-based ECL ratiometric sensors is limited by the lack of energy-tunable materials, especially ECL-RET donors and acceptors that perfectly overlap.

Researchers have introduced a dual-role energy transfer intermediate that integrates the quenching effect and catalytic properties to address the lack of ECL-RET luminophore pairs. Metal nanoparticles (NPs), such as platinum NPs [47] and gold NPs (AuNPs) [34] are the most commonly selected energy transducers because of their different effects on the ECL of CdS and luminol. The most common pattern of the intermediate ECL-RET strategy is constituted by luminol-functionalized AuNPs and CdS-C nanoflowers (NFs) [48]/G-CdTe QDs [42]/CdTe@CdS QDs [23]. The mediatory function of AuNPs comprises (a) the anodic ECL enhancement attributed to the increased active electrode area and the catalytic effect on luminol oxidation [48] and (b) the cathodic quenching resulting in nonradiative energy dispersion or Förster RET from QDs [49]. Additionally, at a certain distance, excited-state QDs could stimulate the surface plasmon resonance of AuNPs, which generates powerful local electric fields and then leads to additional excited-state QDs [50] to enhance the intensity of cathodic ECL. The formation pattern of the dual-role energy transfer intermediate in the ratiometric platform is shown in Figure 1B, in which the binding of target molecules changes the conformation of rigid structures of the DNA chain, thus altering the distance between CdSe/ZnS and AuNPs-luminol such that two ECL signals at different potentials are changed oppositely to form the ratiometric ECL biosensor [51]. At present, many RET-ECL ratiometric systems have been developed on the basis of dual-role intermediates, which include luminol-Str-AuNPs/CdS [52], Au-luminol/CdSe/ZnS QDs [51], luminol-AuNPs/CdS-C NFs [48], luminol/CdTe/CdS/ZnS QDs [39], luminol/CdTe@

CdS QDs [34], Ag-PAMAM-luminol NCs/graphitic carbon nitride (g-C₃N₄) [53], luminol/GQD [24], luminol/CdS NCs [5], and CdTe/CdS/ZnS QDs-HRP/AuNRs-luminol [39].

Nevertheless, the above ECL-RET strategies lack universal applicability because of the demanding requirement for sufficient spectrum overlap between the ECL energy donor and acceptor. Therefore, a universal enhancer or quencher is desirable for dual-potential ratiometric ECL sensors. Wang *et al.* [54] proposed a superior and universal quencher, cuprous oxide (Cu₂O) (Figure 1C). Cu₂O, a p-type semiconductor, has been confirmed to consume dissolved oxygen by catalyzing oxygen reduction during the negative scan and thus could be an effective quencher for luminophores with dissolved O₂ as the co-reactant. Similarly, Fu *et al.* [55] utilized Cu₂O to form a self-enhanced Cu₂O-TAEA-Ru (II) complex as an anodic ECL label and embellished graphene-CdTe QDs as the cathodic ECL probes on the surface of the electrode to develop a dual-potential ECL ratiometric sensor for the sensitive detection of dopamine. The ratiometric detection of dopamine was realized via the ECL-RET from G-CdTe QDs to TAEA-Ru, as well as the dual quenching effects of Cu₂O on G-CdTe QDs, namely, the ECL-RET from G-CdTe QDs to Cu₂O and the consumption of the co-reactant O₂ by Cu₂O. Other intermediates have also been reported by Zheng *et al.* [56], who first utilized ferrocenecarboxylic acid (FCA) as a bifunctional reagent to regulate the ratiometric ECL sensing mode by virtue of the double effects of FCA in quenching the ECL of Ru (dcbpy)₃²⁺ through inhibiting the generation of excited-state Tris (2,2'-bipyridine)Ru (II) (Ru (bpy)₃²⁺) and enhancing luminous efficiency by catalyzing the generation of the reactive oxygen species (ROS, OH· and O₂⁻) that facilitate the oxidation of luminol.

Above all, the ECL-RET strategy is gaining popularity as a potent signal regulation approach in ratiometric ECL systems. Several energy transfer intermediate reagents, including metal NPs, Cu₂O, and FCA, have been widely used. Additional RET luminous pairings with potential resolution qualities will most likely be constructed in the future. Also, finding RET intermediate compounds is essential for solving the lack of effective pairs of energy donors and acceptors and for increasing the number of ECL-emitting systems used in potential-resolved ratiometric systems.

Competition Strategy

In addition to ECL-RET-based potential-resolved systems for establishing ratiometric sensors, systems based on the competitive strategy have been

widely constructed given their inherent superiority in triggering the reverse signal changes of dual potential-resolved ECL emitters [22]. The competitive strategy of co-reactant consumption has been extensively investigated and maturely developed, and more recently, several research contends for the binding space of the electrode surface, known as steric hindrances competition systems, have emerged to form the ratiometric system.

By relying on the different catalytic efficiencies of luminophores for their shared co-reactants, the consumption of competitive co-reactants between a pair of potential-resolved luminophores was utilized for ratiometric ECL sensors [41]. Various competitive co-reactant-consuming ECL ratiometric systems have been constructed on the basis of H₂O₂ because of its combined reducing and oxidizing properties. For example, Fang *et al.* [62] used the self-enhanced glutathione (GSH)-N-(aminobutyl)-N-(ethyl-isoluminol) (ABEI) composite as an anodic probe and labeled the anti-antibody with the cathodic probe

g-C₃N₄ nanosheets (NSs) and horseradish peroxidase (HRP) in a zearalenone (ZEN) immunoassay. When immune recognition occurred, the anodic ECL signal increased and the cathodic ECL signal decreased due to the competitive consumption of the co-reactant H₂O₂ by the g-C₃N₄ NSs and GSH-ABEI (Figure 2A). Furthermore, peroxidase accelerated the decomposition of H₂O₂ into ROS, thus simultaneously amplifying the blue ECL of ABEI and the green ECL of g-C₃N₄ and contributing to the widening of the linear range and the increase in sensitivity [63]. Other luminophore pairs with H₂O₂ as the shared co-reactant, such as LuAuNPs/AuNPs@CNNS [64] and CdS QDs/luminol [33], have been utilized in this ratiometric ECL sensing system. However, several inherent defects in H₂O₂ impede its application in the competitive consumption strategy: (1) H₂O₂ has been identified to be an unstable co-reactant because it is prone to decomposition into OH· radicals at ambient temperature. Furthermore, when present in excess, H₂O₂ molecules may annihilate each other. This

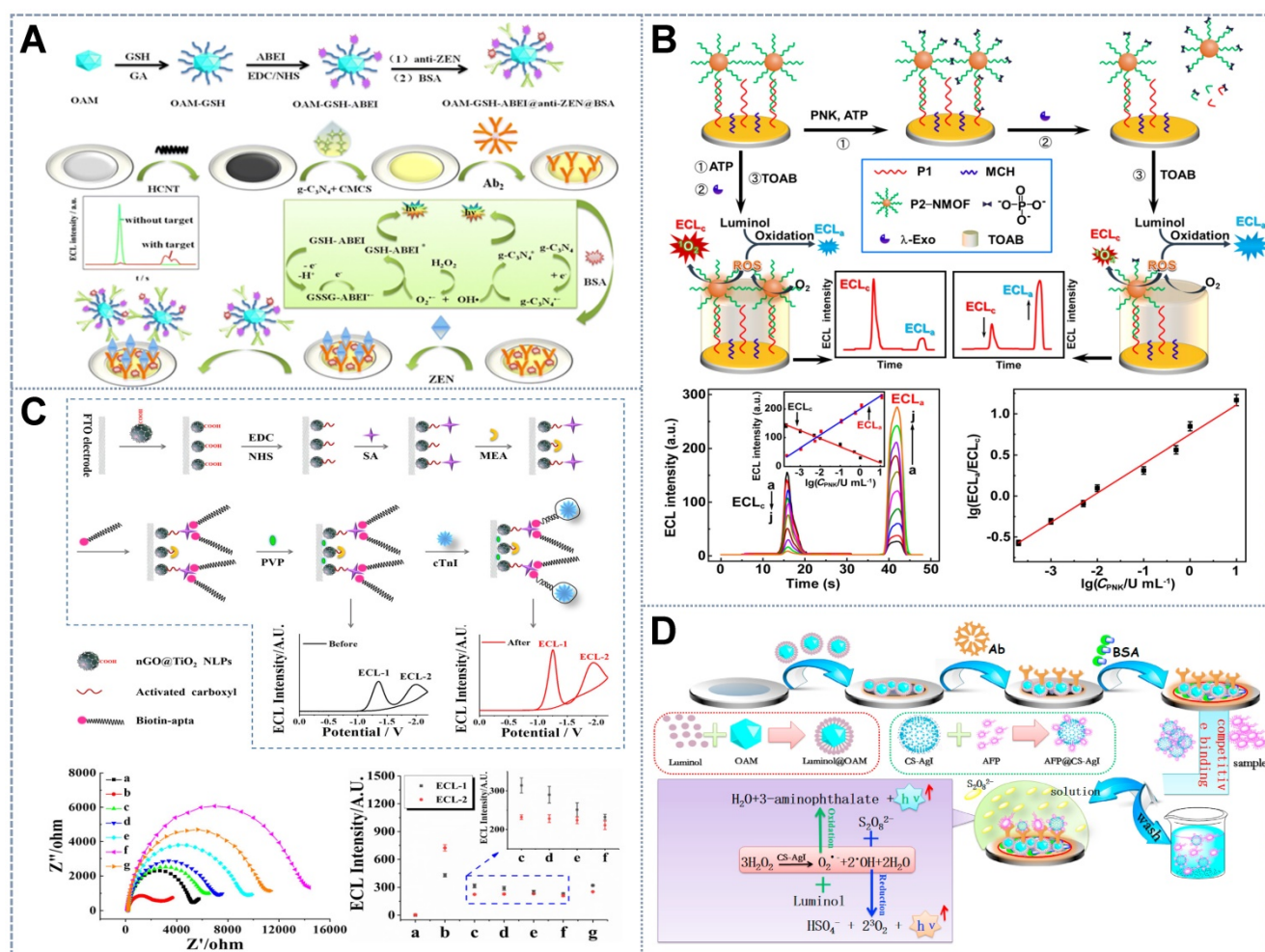


Figure 2. Schematic of potential-resolved competition-strategy sensors with (A) H₂O₂ as the co-reactant. Adapted with permission from [62], copyright 2020 Springer; and (B) dissolved O₂ as the co-reactant. Adapted with permission from [65], copyright 2020 American Chemical Society. (C) Steric hindrance strategy. Adapted with permission from [69], copyright 2019 American Chemical Society. (D) Immune competition mechanism. Adapted with permission from [71], copyright 2016 Elsevier B.V.

phenomenon greatly affects the stability and reproducibility of bioanalysis [65]. (2) H_2O_2 , an exogenous co-reactant, has a relatively low catalytic efficiency that leads to its higher consumption of reagents than the endogenous co-reactants. (3) Given its biological toxicity and volatility, H_2O_2 poses certain safety risks, which will also affect measurement deviation [63]. So, it is very important and could be very useful to look for a stable and green co-reactant for the competitive consumption strategy in ratiometric ECL systems.

Compared with H_2O_2 , dissolved O_2 in aqueous solutions is a more promising endogenous co-reactant candidate, especially in luminol ECL systems, due to its higher stability and nontoxicity. Dissolved O_2 in the solution can be used directly as a co-reactant or can be continuously adsorbed and dissociated at the catalytic interface during the oxygen reduction reaction (ORR) to generate ROS or H_2O_2 for subsequent ECL reactions. Zhang *et al.* [65] proposed a dissolved O_2 -competing ECL catalytic interaction involving two-dimensional copper-based zinc porphyrinic MOF (CuTCPP (Zn))NSs and luminol. The constructed GNPs would diminish the cathodic ECL of the singlet oxygen formed through the electrocatalytic reaction of the two-dimensional CuTCPP (Zn) due to RET, while the GNPs with strong electrocatalytic activity would boost the anodic emission of luminol (Figure 2B). The ECL process driven by the competitive mechanism had a lower detection limit and a broader linear relationship in the detection of polynucleotide kinase (PNK) than single-signal-driven ECL sensors due to the participation of dissolved O_2 . The same dissolved O_2 competing system with the anodic emitter ABEI, the cathodic emitter CdTe QDs [66], and 2-(dibutylamino) ethanol (DBAE)/lucigenin [67] demonstrated excellent stability, selectivity, and reproducibility. The co-reactant competitive ratiometric ECL mechanism based on dissolved O_2 or its products may provide a new pathway for further research on green and highly sensitive ECL biosensing systems.

The steric hindrance competition strategy has been introduced into ratiometric ECL systems with multiple recognition modes in an effort to form ultrasensitive and economical target-mediated self-calibrated ECL sensors. For example, on the basis of a molecularly imprinted (MIP) recognition platform, Cao *et al.* [68] constructed a simple and universal steric hindrance ratiometric ECL sensor with TiO_2 -Ru(bpy) $_3^{2+}$ NPs as the anodic luminophore and PEI-CdS QDs as the cathodic luminophore and anodic co-reactant, thus avoiding the addition of multiple co-reactants. The SA-imprinted poly[3-aminophenylboronic acid] film was prepared on

the electrode as the recognition element and then modified with two luminophores, which strictly hindered electron transfer and impeded the direct contact of the cathodic co-reactant H_2O_2 with PEI-CdS. After the binding, elution, and re-recognition of SA on the MIP, the sensor exhibited an obvious increase in the intensity of the ECL signal from Ru(bpy) $_3^{2+}$ and an evident decline in the intensity of the ECL signal from PEI-CdS because SA could assist the ECL reaction of Ru(bp) $_3^{2+}$ by acting as an anodic co-reactant and the cathodic reaction was impeded by the occupation of the imprinted cavities. Furthermore, Han *et al.* [69] applied the steric hindrance strategy based on a label-free ECL aptasensor for the determination of cardiac troponin I (cTnI) (Figure 2C). In this sensor, the dual-signal nanoluminophore nanographene oxide (nGO)-wrapping titanium dioxide (nGO@TiO $_2$ NLPs) that was fabricated on the ECL interface generated two potential-separated ECL. Aptamers for cTnI assembled on nGO@TiO $_2$ NLP for target capture. After binding with cTnI, the aptamer becomes too rigid to cling to the surface of the electrode, thus leaving space for charge transfer. This effect resulted in the ratio enhancement of the two ECL signals of nGO@TiO $_2$ NLPs. Interestingly, Wang *et al.* [70] introduced a catalyzed hairpin assembly-driven bipedal DNA walker into the ratiometric strategy to form the Au@luminol-HP1/Au@CDs-HP2 duplex on the sensing interface. After the introduction of Au@CDs-HP2 into the electrode-bound Au@luminol-HP1 hairpins, a cathodic ECL signal was observed as a result of the addition of Au@CDs, and the anodic ECL signal decreased because steric hindrance from the Au@CDs-HP2 complex blocked the interaction between Au@luminol and H_2O_2 . By exploiting the high luminescence and excellent biocompatibility of AuNPs/luminol and AuNPs/carbon dot hybrids, the proposed system exhibited superb ratiometric performance and also offered a reliable method for early clinical diagnostics and cutting-edge biomedical research.

The target-involved competitive immunoassay, another competitive ratiometric system, is a promising sensing protocol because of its minimalist design and ultrasensitive determination. Zhang *et al.* [71] constructed an enzyme-labeling competitive immunoassay for determining alpha fetoprotein (AFP). The immunorecognition interface was constructed by incubating the mixture solution of chitosan-functionalized silver iodide (CS-AgI)-labeled AFP (CS-AgI@AFP) and the target AFP on the antibody (Figure 2D). With the increase in the concentration of AFP, the amount of the CS-AgI@AFP immobilized on the electrode decreased due to the competitive recognition of AFP, resulting in the reduced catalytic

effect of CS-AgI for the decomposition of H₂O₂. This effect consequently amplified the potential-resolved ECL of luminol and S₂O₈²⁻ in the ratiometric ECL strategy. The proposed competitive immunoassay omitted the introduction of secondary antibodies, thus facilitating electrode transfer on the recognition platform and guaranteeing its outstanding sensitivity over the common sandwich immunoassay.

Enzyme-based Ratiometric Strategy

The potential-resolved enzyme-based ratiometric strategy is an enzyme-catalyzed ratiometric method. It exploits the enzymatic reactions between the reactant and product, which act as the co-reactants of two different ECL emitters, to attain the distinguishable changes in the potentials of inverted ECL signals for ratiometric determination. This platform possesses excellent accuracy, reliability, and sensitivity and is therefore an alternative for alleviating the shortage of suitable luminous pairs, the limitation of the distance dependence of RET, and the cross-talks between co-reactants in luminating systems [74]. Various types of enzymes, especially oxidoreductases, such as the acetylcholinesterase (AChE)-ChOx enzyme system and xanthine oxidase (XOD), have been utilized to catalyze the production and consumption of ECL signal regulators, including O₂ and H₂O₂, to realize signal conversion. Chen *et al.* [75] integrated two desirable ECL emitters, namely, polymer poly(9,9-dioctylfluorene) (PFO) dots and

CdTe QDs, that feature ideal properties, such as potential-resolved ECL signal emission and freedom from mutual energy transfer. The PFO dots and CdTe QDs took the enzymatic reaction reactant dissolved O₂ and product H₂O₂ as their exclusive co-reactants, respectively (Figure 3A). Such a construction strategy overcomes the limitations of using exogenous co-reactants and the discommodity of oxidase-based determination in the traditional ECL ratiometric method. However, given that the luminous efficiency of this system suffered from the poor water solubility of PFO, the same group established another anodic luminophor luminol with favorable water solubility by using H₂O₂ as the co-reactant for the determination of the XOD substrate hypoxanthine (Hx) [76]. In the presence of Hx, XOD catalyzed oxidation, resulting in the *in situ* consumption and generation of dissolved O₂ and H₂O₂, which served as the co-reactants of rGO-CdTe QDs and luminol, respectively. This phenomenon resulted in the reduction of the cathodic signal and the enhancement of the anodic signal, upon which Hx was ratiometrically detected with a low detection limit. The *in situ* consumption and generation of co-reactants via enzyme catalysis not only offered an ingenious tactic for the determination of substrate concentration but also alleviated the error introduced by exogenous co-reactants in common ratiometric systems.

Table 2. Summary of the partial reports on potential-resolved ratiometric ECL analysis based on the competition strategy. Unavailable measurements are represented by "--"

Competition strategy	Pairs of luminophores	Linear range	LOD	Target	Ref.
H ₂ O ₂	LuAuNPs/ AuNPs@CNNS	1.0 × 10 ² –1.0 × 10 ⁶ cells/mL	20 cells/mL	Circulating tumor cells and cell-surface glycans	[41]
O ₂	Zinc tetrakis [carboxyphenyl]-porphyrin/luminol	2.0 × 10 ⁻⁴ –10 U /mL	6.5 × 10 ⁻⁵ U/mL	PNK	[65]
	CdTe QDs/ABEI	1.0 × 10 ⁻¹³ –1.0 × 10 ⁻⁸ g/mL	3.0 × 10 ⁻¹⁴ g/mL	Concanavalin A	[2]
	DBAE/lucigenin	1.0 × 10 ⁻¹⁴ –1.0 × 10 ⁻⁸ g/ml	3.3 × 10 ⁻¹⁵ g/mL	Human epididymis protein 4	[67]
H ₂ O ₂	CdS QDs/luminol	1.0 × 10 ⁻¹² –1.0 × 10 ⁻¹⁰ g/ mL	6.2 × 10 ⁻¹³ g/mL	Carcinoembryonic antigen A	[33]
	ABEI/g-C ₃ N ₄	1.0 × 10 ⁻¹³ –1.0 × 10 ⁻⁸ g/mL	3.3 × 10 ⁻¹⁴ g/mL	Zearalenone	[63]
Steric hindrance	TiO ₂ -Ru(bpy) ₃ ²⁺ NPs/PEI-CdS QDs	1.0 × 10 ⁻⁹ –1.0 × 10 ⁻⁴ M	1.7 × 10 ⁻¹¹ M	SA	[68]
	nGO@TiO ₂ NLPs/K ₂ S ₂ O ₈	1.0 × 10 ⁻¹³ – 1.0 × 10 ⁻¹⁰ M	4.0 × 10 ⁻¹⁴ M	cTnI	[69]
	Au@CDs NFs/ Au@luminol NPs	1.0 × 10 ⁻¹⁵ –1.0 × 10 ⁻¹¹ M	3.4 × 10 ⁻¹⁶ M	p53 DNA	[70]
Competitive immunoreaction	Luminol/CS-AgI	1.0 × 10 ⁻¹⁵ –2.0 × 10 ⁻⁸ g/mL	1.0 × 10 ⁻¹⁵ g/mL	AFP	[72]
H ₂ O ₂	Ir NRs/CdS QDs	5.0 × 10 ⁻¹² –5.0 × 10 ⁻⁸ M	1.67 × 10 ⁻¹² M	EP	[73]
O ₂	Luminol/Cu-TCPP [Zn]	5.0 × 10 ⁻³ –5.0 U/mL	3.7 × 10 ⁻³ U/mL	Protein kinase A	[49]

Table 3. Summary of the partial reports on potential-resolved ratiometric ECL analysis based on enzymes. Unavailable measurements are represented by "--"

Enzyme	Pairs of luminophores	Linear range	LOD	Target	Ref.
AChE	rGO-CdTe QDs/PFO dots	5.0 × 10 ⁻¹³ –1.0 × 10 ⁻⁸ M	1.25 × 10 ⁻¹³ M	OPs	[75]
	c-PFBT NPs/L-CdS QDs	5.0 × 10 ⁻¹³ –5.0 × 10 ⁻⁷ M.	1.25 × 10 ⁻¹³ M	EP	[81]
XOD	rGO-CdTe QDs/luminol	2.0 × 10 ⁻¹¹ –2.0 × 10 ⁻³ M	7.0 × 10 ⁻¹² M	Hx	[63]
HRP	ABEI/GSH	1.0 × 10 ⁻¹³ –1.0 × 10 ⁻¹² g/mL	3.3 × 10 ⁻¹⁴ g/mL	ZEN	[71]
CS-AgI	Luminol/K ₂ S ₂ O ₈ /CS-AgI	1.0 × 10 ⁻¹⁵ –2.0 × 10 ⁻⁸ g/mL	1.0 × 10 ⁻¹⁵ g/mL	AFP	[82]
GOx	PFO NPs	5.0 × 10 ⁻¹⁷ –1.0 × 10 ⁻¹⁰ M	1.7 × 10 ⁻¹⁷ M	miRNA-155	[80]

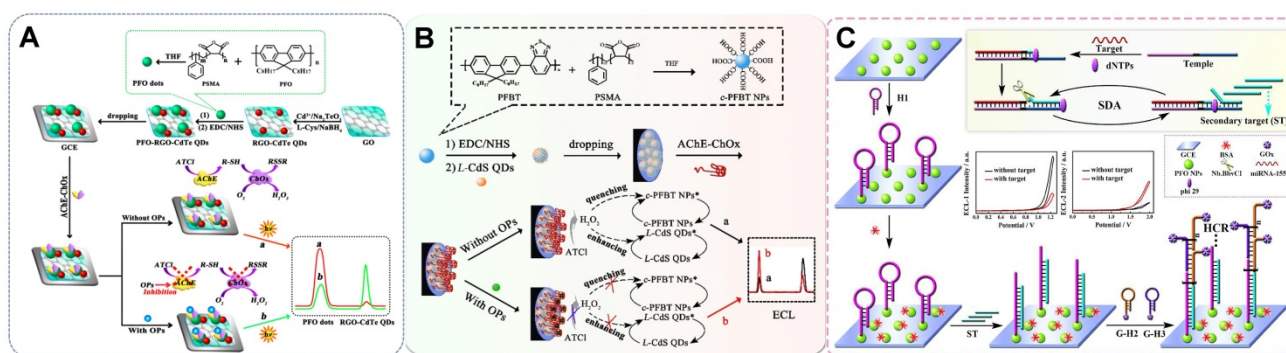


Figure 3. Schematic of the potential-resolve enzymatic strategy sensors based on the reverse variation of the substrate O_2 and H_2O_2 in (A) the AChE-ChOx enzyme system. Adapted with permission from [75], copyright 2017 American Chemical Society; single H_2O_2 substrate as the bifunctional moderator in (B) the glucose oxidase system. Adapted with permission from [74], copyright 2020 Elsevier B.V.; and (C) the AChE system. Adapted with permission from [81]. Copyright 2021 American Chemical Society.

Other commonly constructed enzyme ratiometric sensors are based on single H_2O_2 . H_2O_2 could serve as a bifunctional moderator to mediate the opposite change of the two signals because it is taken as a substrate or product in various enzymatic reactions [77–79]. For example, Zhang *et al.* [80] designed metal-organic gel catalyst Fe(III)–organic gel matrices for the efficient enhancement of the ECL signals of luminol and CdS QDs through the conversion of the co-reactant H_2O_2 into ROS via an electrochemically mediated Fenton-like reaction. A dual-potential ratiometric strategy was proposed for the accurate cytosensing and direct evaluation of VEGF₁₆₅ subtypes on cell surfaces. Taking advantage of the quenching and enhancing adverse regulatory effect of H_2O_2 produced by GOx, Liu *et al.* [74] achieved the ratiometric sensing of miRNA-155 on the basis of the ratio of two ECL signals emitted by PFO NPs at two potentials (+1.25 and +1.95 V) (Figure 3B). Similarly, He *et al.* [81] developed a bifunctional moderator-powered enzymatic biosensor based on a dual-signal combined nanoprobe and the enzyme AChE. In this system, AChE catalyzed the substrate acetylthiocholine to produce H_2O_2 , which quenched the anodic ECL signal from c-PFBT NPs and promoted the emission of the cathodic ECL signal from L-CdS QDs for organophosphorus analysis (Figure 3C). Taking into account the problems with RET and exogenous co-reactants, the above-mentioned enzymatic biosensors avoided the troublesome step-by-step assembly of two signal probes in ECL sensor and also provided a new measure for facilitating the opposite changes of two signals.

The enzyme-labeling amplification strategy has been proven to intensify ECL signals in ratiometric ECL protocols to improve the sensitivity of ECL detection. Fang *et al.* [63] labeled anti-ZEN with HRP, which accelerated the decomposition of H_2O_2 into ROS, thus significantly amplifying the potential-

resolved ECL signal of ABEI and GSH. This effect facilitated sensitive and reliable ZEN analysis with a wide linear range in corn hazelnut samples. Nevertheless, the generalization of the enzyme-labeling strategy is impeded by some intrinsic drawbacks, such as expensive preparation and purification processes, environmental susceptibility, and undesirable stability. Artificial enzyme mimics have received widespread attention because of their alternative catalytic activities for signal amplification and high stability, reasonable cost, spatial structure flexibility, and storage stability. Zhang *et al.* [71] utilized the biomimetic catalyst CS–AgI to catalyze the decomposition of H_2O_2 into O_2^- and $\cdot OH$, which served as the co-reactants of the potential-resolved emitters luminol and $K_2S_2O_8$, respectively. This approach resulted in the enhancement of dual ECL responses. The enzyme-triggered amplification protocol provides a promising strategy for improving the sensitivity of potential-resolved dual-electrode reaction systems, and its application in visualized detection has a bright future.

Single Luminophore Ratiometric ECL Strategy

Although the reported conventional ratiometric ECL systems based on ECL–RET, competitive strategy, or enzymatic reactions have provided more reliable and sensitive sensing signals than those based on traditional single emitters, they mainly require two elaborately selected potential-resolved luminophores and complex combinations of co-reactants, as well as multiple assembly steps and labeling courses. Existing studies have found that many single luminophores can produce dual ECL signals under the application of different potentials and in the presence of corresponding co-reactants [83]. Through the reasonable design of the sensing interface, these luminescence systems could considerably expand the ratiometric ECL strategy.

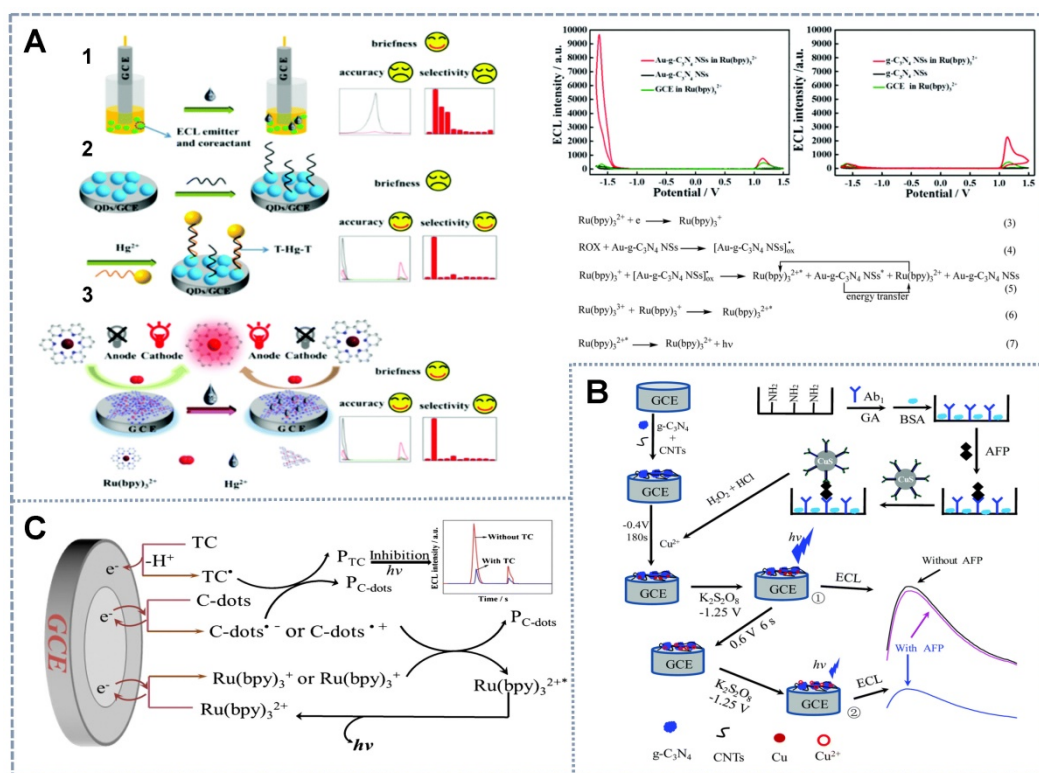


Figure 4. Schematic of single luminophore ratiometric ECL sensors based on dual co-reactants. **(A)** G-C₃N₄ and Au-g-C₃N₄ as the co-reactants of Ru(bpy)₃²⁺ for Hg²⁺ detection. Adapted with permission from [84], copyright 2020 Royal Chemical Society. **(B)** K₂S₂O₈ and TEA as the co-reactants of porous g-C₃N₄ NSs for AFP detection. Adapted with permission from [53], copyright 2020 Royal Chemical Society. Single-luminophore ratiometric ECL sensors based on **(C)** C-dots as the single co-reactant of Ru(bpy)₃²⁺ for the determination of the antibiotic TC. Adapted with permission from [87], copyright 2019 Springer.

Table 4. Summary of the partial reports on potential-resolved ratiometric ECL analysis based on single luminophores. Unavailable measurements are represented by “–”

Luminophor	Co-reactant	Linear range	LOD	Target	Ref.
Ru(bpy) ₃ ²⁺	Au-g-C ₃ N ₄ NSs	5.0 × 10 ⁻¹⁰ –5.0 × 10 ⁻⁷ M	2.0 × 10 ⁻¹⁰ M	Hg ²⁺	[84]
NGQDs	O ₂ ⁻ /HO ₂ ⁻	1.0 × 10 ⁻³ –7.0 × 10 ⁻² M	2.0 × 10 ⁻⁴ M	Co ²⁺	[85]
g-C ₃ N ₄	K ₂ S ₂ O ₈ /TEA	3.0 × 10 ⁻¹⁶ –1.0 × 10 ⁻¹¹ g/mL	1.0 × 10 ⁻¹⁶ g/mL	AFP	[53]
Ru(bpy) ₃ ²⁺	C-dots	1.0 × 10 ⁻⁹ –1.0 × 10 ⁻⁴ M	4.7 × 10 ⁻¹⁰ M	TC	[87]

The special properties of the electrochemical reaction between the analyte and the dual-signal single luminophore are mainly utilized via an ingenious design to realize the construction of ratiometric determination systems. Due to their high quantum efficiency and anodic or cathodic ECL emission properties upon reaction with different co-reactants, Ru(bpy)₃²⁺ and its derivatives are the most widely used ECL emitters in single luminophore-based ratiometric systems. However, the lack of modifiable cathodic co-reactants impedes their application. Cao *et al.* [84] proposed the novel cathodic co-reactant Au-g-C₃N₄ NSs of Ru(bpy)₃²⁺ (Figure 4A) prepared via the in-situ synthesis of AuNPs on the surface of g-C₃N₄ NSs, which is the anodic co-reactant of Ru(bpy)₃²⁺. They utilized the formation of gold amalgam between Hg²⁺ and Au to develop a label-free Hg²⁺ ratiometric sensor by inhibiting the activity of AuNPs. This effect simultaneously hindered cathodic ECL emission and

enhanced anodic emission. Furthermore, Chen *et al.* [85] synthesized the single-emitter nitrogen-doped graphene QDs (NGQDs) by using the oxygen electrolytic products O₂⁻ and HO₂⁻ under positive and negative potentials as the anodic and cathodic co-reactants, respectively, to produce bipotential responses. Then, the Co²⁺ ion was determined on the basis of the amplification of the anodic signal by the catalytic action of Co²⁺ during the intermediate steps of the anodic ECL process and the quenching of the cathodic ECL intensity due to the Co²⁺ elimination effect of the excited state (NGQDs^{*}) generation. In addition, Shang *et al.* [86] reported that dual-ECL signals could be generated by distinct ECL reactions triggered by GPPCN NSs at anodic and cathodic potentials to distinguish trace amounts of target metal ions when the concentrations of interfering metal ions were several times higher. At different driving potentials, different metal ions showed variable signal quenching and enhancement likely due to the

diversity of the energy level matching between metal ions and GPPCN NSs and the catalytic interactions of the intermediate species in ECL reactions. As a result, the accuracy and reliability of sensors based on the ECL of GPPCN NSs for metal ion detection were considerably enhanced, the need for any labeling or masking reagents was eliminated, and the production of false-positive results by interferential metal ions was effectively prevented. Therefore, using the special chemical reactions between different metals and ECL materials, it is possible to measure the amount of metal ions with high sensitivity and selectivity from the ratio of two ECL signals at different potentials.

The proposed strategy for the construction of sensing interfaces based on signal emitters could be utilized not only for the detection of metal ions but also for the determination of large molecules, such as proteins, aptamers, and even cells with complex designs. Labels and substrates with potential discrimination properties without the chemical characteristics of metal elements are needed for the detection of biomaterials. Chen *et al.* [53] reported a biometallization signal amplification strategy. In this strategy, porous $g\text{-C}_3\text{N}_4$ NSs were used as the single luminophore with $\text{K}_2\text{S}_2\text{O}_8$ and triethanolamine (TEA) as the cathode and anode co-reactants (Figure 4B), and CuS NPs were applied as the tag to build an ultrasensitive immunoassay for AFP detection. Specifically, the sensing interface consisted of $g\text{-C}_3\text{N}_4$ NS-modified carbon nanotubes (CNTs) as the electrode base and second antibodies labeled by CuS NPs as the probe. The ECL determination process was coupled with the anodic stripping voltammetry strategy to amplify the ECL signals of the electrochemical deposition of Cu from the CuS NP tag at a negative potential and the dissolution and enrichment of Cu^{2+} within the Helmholtz layer of GCE/CNTs- $g\text{-C}_3\text{N}_4$ at a positive potential that significantly quenched the $g\text{-C}_3\text{N}_4$ emission. The cathodic signal was taken as the internal reference, and the anodic signal that changed reversibly with AFP was quantified by using a ratiometric ECL system. The combination of ratiometric ECL with electrochemical enrichment and biometallization is a useful strategy for enhancing the sensitivity and reproducibility of immunoanalysis.

Another strategy relies only on a single emitter and a single co-reactant to attain the simplest ratiometric ECL system. In this system, the ratio of the dual signal with a single-directional change at separate potentials was used as the output signal. For the detection of the antibiotic tetracycline (TC), Hu *et al.* [87] employed $\text{Ru}(\text{bpy})_3^{2+}$ as the single electrochemical probe that exhibited a double ECL response with potential scanning from -3.5 V to $+2$ V

and C-dots as the co-reactant (Figure 4C). The dual signals of $\text{Ru}(\text{bpy})_3^{2+}$ decreased with the increase in TC concentration due to the inhibitory effect of C-dots on TC during the electrochemical reaction. Similarly, Han *et al.* [69] reported the new core-shell-like structured nanoluminophore $n\text{GO@TiO}_2\text{NLPs}$. The $n\text{GO@TiO}_2\text{NLPs}$ were synthesized through a one-pot hydrothermal method and exhibited potential-resolved property with the co-reactant $\text{K}_2\text{S}_2\text{O}_8$ at $\text{pH} = 7.0$. The peak potentials of ECL-1 and ECL-2 were observed at -1.27 and -1.85 V and were emitted by the TiO_2 and $n\text{GO}$ moieties of the $n\text{GO@TiO}_2$ NLPs, respectively. After the addition of the target cTnI, the dual signal was simultaneously quenched due to the steric hindrance of the aptasensor. On the basis of the ratio of ECL-1 and ECL-2 intensities, a label-free ratiometric ECL system was constructed for the detection of the AMI biomarker cTnI. The system enabled the superior, accurate, sensitive, specific, and rapid early detection of AMI. Therefore, the exploitation of the dual-signal strategy based on one luminophore has a bright future given its economy, environmental friendliness, and simple system construction.

Internal Standard Ratiometric Sensing Strategy

The internal standard ratiometric sensing strategy is another protocol for constructing a ratiometric signal-based sensing platform in conjunction with the dual-potential based strategy mentioned above. While in the internal standard ratiometry scheme, exploiting the ECL luminophore pair to generate differentiable ECL working signal and internal reference in one single scan is a key factor. Thus the potential-resolved ECL system is the foundation stone of internal reference ratiometric sensors [88].

The internal standard ratiometric strategy was initially realized on the basis of physically separated double disk electrodes (WE1 and WE2). The mechanism of the internal reference scheme on spatial-resolved disks is based on the self-calibration of the ratio of ECL signals from WE1 (as the working signal) to WE2 (as the internal reference standard signal). Feng *et al.* [89] fabricated an internal standard ratiometric aptasensor on a homemade screen-printed carbon electrode (SPCE) for the detection of the antibiotic chloramphenicol (CAP) for the first time. The working signals from the anodic luminophore Lu-AuNPs were compared with the internal standard signals from CdS QDs at negative potential to reduce environmental disturbance. Cao *et al.* [90] presented a novel dual-disk inner reference ratiometry method for cTnI analysis (Figure 5A). WE1 and WE2, which were

considered as the working and reference electrodes, respectively, were modified with CdS nanowires (CdS NWs) as the potential-resolved cathodic emitter and luminol–AuNPs (L–AuNPs) as the anodic emitter. Dual-signal-amplifying probe anti-cTnI-reduced graphene oxide–AuNPs–catalase loaded onto the WE1 functioned as the RET acceptor of CdS NWs and as the CAT catalyzing the co-reactant (i.e., H₂O₂) consumption that resulted in a prominent decrement in ECL along with an increase in cTnI concentration. Internal and external interferences were remarkably calibrated by the internal reference signal from WE2 loaded with L–AuNPs embedded with a fixed amount of cTnI. Furthermore, the physical separation of the workspaces of different emitting systems conspicuously mitigated the potential cross-talk and cross-reactivity between luminophores, thus

effectively increasing the specificity and reliability of ECL performance. Wang *et al.* [88] designed a label-free spatial-resolved dual-signal-output ratiometric biosensor based on a dual-disk glassy carbon electrode (DDCE) for the prostate-specific antigen (PSA) assay (Figure 5B). Self-synthesized three-dimensional flower-like CdS assemblies were used as the cathodic ECL emitters. Ru(bpy)₃²⁺@RuSi NPs, which acted as the anodic ECL emitter, emitted the working signal that served as the reference signal to alleviate environmental interference during biological recognition. The exact same building process and unified building pattern between the two disks universally endowed the dual-disk electrode-based internal standard ratiometric strategy with an ultra-accurate and reliable biosensing scheme.

Table 5. Summary of the partial reports on potential-resolved ratiometric ECL analysis based on the internal standard strategy. Unavailable measurements are represented by "–"

Luminophor	Tag	Linear range	LOD	Target	Ref.
Internal standard strategy based on a single electrode					
L–AuNPs/CdS NWs	cTnI–rGO–AuNPs–CAT	5.0 × 10 ^{–13} –1.0 × 10 ^{–7} g/mL	1.0 × 10 ^{–13} g/mL	cTnI	[89]
L–AuNPs/CdS QDs	CA	1.0 × 10 ^{–10} –1.2 × 10 ^{–7} M	3.0 × 10 ^{–11} M	CAP	[90]
Internal standard strategy on double disk electrode					
Substrate/internal reference	Label emitter	Linear range	LOD	Target	Ref.
Luminol	CdTe QDS	1.0 × 10 ² –6.5 × 10 ³ cell/mL	80 cell/mL	MCF-7 cells	[93]
Au@Luminol	CIZS/ZnS QDs	1.0 × 10 ^{–14} –1.0 × 10 ^{–9} M	1.82 × 10 ^{–15} M	Thrombin	[94]
g–C ₃ N ₄	Pdots	1.0 × 10 ^{–14} –1.0 × 10 ^{–8} g/mL	3.3 × 10 ^{–15} g/mL	Human epididymis protein 4	[32]

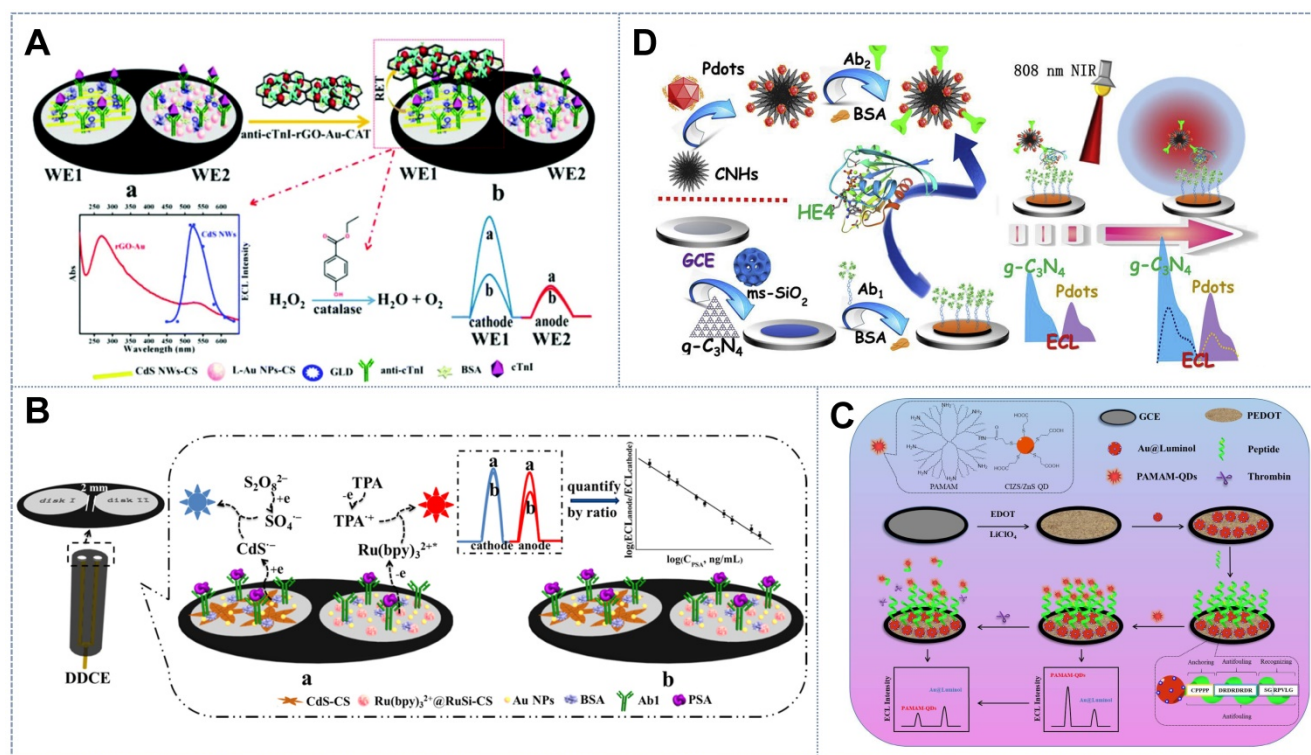


Figure 5. Schematic of the internal standard ratiometric ECL sensor with the physically separated double disk electrode (WE1 and WE2) in (A) a dual-disk inner reference ratiometry system. Adapted with permission from [90], copyright 2020 Royal Chemical Society; (B) a DDCE label-free system. Adapted with permission from [88], copyright 2017 Elsevier B.V. Schematic of the internal standard ratiometric ECL sensor with the physically separated double disk electrode (WE1 and WE2) with single electrode assembled with an internal reference signal probe and working signal probe in (C) a ratiometric antifouling ECL biosensor based on PAMAM-CIZS/ZnS QDs. Adapted with permission from [91], copyright 2020 Elsevier B.V.; and (D) with photothermal amplification strategies. Adapted with permission from [32], copyright 2019 Elsevier B.V.

Further studies assembled the internal reference signal and working signal in one electrode as a concise construction mode to generalize the internal standard ratiometric sensing strategy to a common single-disk electrode. The ratio of dual potential-resolved signals could be acquired for target concentration quantification in the single-sensing interface by modifying one emitter to act as the electrode substrate and internal reference and modifying another potentially distinguishable emitter on the bioprobe as the working signal tag. The favorable accuracy, reliability, and sensitivity of the bioassay were thus realized. Xu *et al.* [91] constructed a ratiometric antifouling ECL biosensor based on the novel benign water-soluble self-enhanced luminescence probe PAMAM-CuInZnS/ZnS QDs (PAMAM-CIZS/ZnS QDs) (Figure 5C). The electrode was modified with the anodic ECL emitter Au@Luminol as the internal standard molecule. The noble metal AuNPs could also simultaneously improve the conductivity of the electrode. Ding *et al.* [92] designed a bimodal ECL system based on CdTe QDs and luminol as the potential-resolved luminophores. CdTe QDs were tagged onto aptamers for cancer cell capture, while luminol molecules, which served as the internal standards, were entrapped in the conducting polymer hydrogel on the electrode surface. In further research, Fang *et al.* [32] introduced photothermal amplification strategies into the internal reference ratiometric ECL system to enhance ECL signals. To do so, the cathodic ECL emitter complex $g\text{-C}_3\text{N}_4@\text{ms-iO}_2$ was designated as the sensing platform and the anodic ECL emitter complex polymer dots (Pdots)@CNH was designated as the photothermal probe (Figure 5D). In this approach, CNHs were used as the thermal conversion unit to increase the electrode surface temperature given their exceptional photothermal property at 808 nm. This effect can convert laser energy into heat for temperature elevation, thus further amplifying the ECL signal. Above all, through incorporation with the internal standard strategy, the developed potential-resolved based ratiometric ECL sensor exhibited satisfactory accuracy, reliability, and practicality in complex biological media. These properties verified its promising utilization in home healthcare and early clinical diagnosis.

Potential-resolved Strategy in Multiplex ECL Analysis

The simultaneous detection of multiple markers in the same sample requires the detection of multiple targets in a single run or in the same system. This approach has more advantages, such as smaller sample volume, lower cost, higher analysis

throughput, and the ability to acquire more information from one sample, than single-target detection [95,96]. Furthermore, the detection of multiple biomarkers is vital for improving the sensitivity and accuracy of cancer diagnosis because tumor markers and tumors lack one-to-one correspondence but instead present complex correlations and stage-dependent differences [97,98]. Therefore, the detection of multiple biomarkers has received increased attention, and additional novel designs have been rapidly developed.

In the potential-resolved strategy, ECL probe signals correspond to each onset working potential. Therefore, the concentration of multiple biomarkers can be revealed through only a simple potential scan of the same sensing interface when it is labeled with different signal probes. Such an approach is timely and convenient. This detection method is called potential-resolved multiplex ECL detection [99]. In contrast to the ratiometric potential-resolved system, some conventional ECL systems are inapplicable to multiplex ECL detection. In these systems, ECL signals are produced by one luminophore with different co-reactants or with a single co-reactant in different chemical states [87]. Therefore, the concentration of ECL probes is not independently linearly related to ECL intensity. Some specific properties need to be met to obtain an accurate and feasible potential-resolved multimarker ECL analysis system without signal interference: (1) Each luminophore should have a separate ECL response that is potentially and originally independent. (2) RET and chemical reaction cross-talk should not exist between luminescent systems. (3) Co-reactants must not interfere with each other.

Luminophore-Co-reactant Pairs in Simultaneous Multimarker Detection

Bilateral Anodic-and-Cathodic Potential Luminescence

Luminophores of vastly different excitation potentials should be chosen for multiplex ECL assays to avoid the overlapping and indistinguishability of two ECL peaks and to enable the complete resolution of the concentration information of multiple markers. Therefore, an anode luminophore, such as luminol and Ru-related complexes [88], and a cathode luminophore, such as QDs [18,45], perylene tetracarboxylic acid, and $g\text{-C}_3\text{N}_4$ [5,100], are usually applied in previously reported potential-resolved multilabel ECL biosensors. Zhao *et al.* [99] constructed a novel potential-resolved ECL strategy based on the luminophore pair ABEI/ O_2 (+0.7 V) and $g\text{-C}_3\text{N}_4/\text{S}_2\text{O}_8^{2-}$ (-1.5 V). Their emission potentials can be clearly distinguished, and no RET occurred between

them. Given the absence of cross-interference and competition between ABEI's co-reactant dissolved oxygen and $g\text{-C}_3\text{N}_4$'s co-reactant $\text{K}_2\text{S}_2\text{O}_8$, ABEI and $g\text{-C}_3\text{N}_4$ have become an ideal combination for multimarker detection. Similarly, Liu *et al.* [26] introduced the luminol analogue 8-amino-5-chloro-7-phenylpyrido(3,4-d)pyridazine-1,4(2H,3H)-dione (L012)(+0.6 V) and $g\text{-C}_3\text{N}_4$ (-1.2 V) as a luminophore pair to construct a new *in situ* detection system for the degree of cell apoptosis, which is induced by the reduction in the expression of epidermal growth factor receptor (EGFR) and the increased eversion of phosphatidylserine (PS) on the cell membrane (Figure 6A). Epidermal growth factor and the peptide PSBP were functionalized with Au@L012 and $g\text{-C}_3\text{N}_4$ as the ECL probes for the recognition of EGFR and PS expression on the cell surface. Thus, the degree of apoptosis was clearly reflected by the change in the two well-separated ECL signals from $g\text{-C}_3\text{N}_4$ and Au@L012. This strategy therefore provides an accurate and reliable way to investigate apoptosis. Similarly, by employing analogical emitters, Liu *et al.* [101] introduced a hollow Cu/Co MOF with effective catalytic performance and loading capacity to construct an ECL aptasensor for the simultaneous detection of acetamiprid and malathion. In this system, luminol and $g\text{-C}_3\text{N}_4$ NSs were used as the signal probe (Figure 6B). The hollow Cu/Co MOF was applied to load the luminol and significantly improved the ECL signal by catalyzing H_2O_2 to produce additional $\text{O}_2^{\bullet-}$. Meanwhile, the material's conductivity was effectively guaranteed because electron mass transfer resistance was avoided by the low density of Cu/Co MOFs. The constructed ECL aptasensor not only eliminated cross-talk between luminescent systems but also exhibited the excellent specificity and sensitivity of 0.015 and 0.018 pM (S/N = 3), respectively, and a low detection limit. The integration of anodic and cathodic ECL luminophores effectively expanded the potential window, which is crucial for improving resolution for ECL multiple target determination. Moreover, highly distinguishable anodic-and-cathodic on-set potential luminophore pairs have been developed ingeniously and flexibly to achieve the simultaneous detection of single cells and cell surface markers. He *et al.* [102] proposed a novel strategy that used capture DNA-hybridized aptamers intercalated with $\text{Ru}(\text{phen})_3^{2+}$ ECL probes to detect cancer cells at positive potential and that applied concanavalin A-conjugated AuNP-modified graphite- C_3N_4 to evaluate N-glycan at the cell surface at negative potential. The ratio of the ECL intensity between the negative potential and positive potential ($\Delta\text{ECL}_n/\Delta\text{ECL}_p$) enabled simultaneous cytosensing and cell

surface N-glycan evaluation. This situation significantly facilitated the understanding of the biological processes related to complex native glycan and promoted the elucidation of N-glycan-related diseases and the clinical diagnosis of physiological processes.

Unilateral Low-potential Luminescence

As described above, given the limited potential scanning window and the easy overlapping of luminous peaks, luminophore pairs with independent ECL at the anode and the cathode are generally adopted to improve resolution strategies. However, the majority of anodic and cathodic ECL luminophores need different co-reactants, and their inevitable side reactions over a wide potential scan interfere with the ECL process [103]. Potential-resolved luminophore pairs sharing the same co-reactant and emitting over a narrow potential scan (i.e., the single anodic or cathodic scan) are preferred given the above issues. Earlier studies focused only on a few types of these multiplex systems given their following limitations: (1) The potential window tolerable for bioassays is relatively narrow, whereas the complete potentially distinguishable multiple ECL signals under single anodic or cathodic scanning usually extends to fairly high voltages because of the wide triggering-potential peak of some ECL luminophores [16]. (2) Although many ECL luminophores, such as cyclometalated Ir (III)/Ru(II) complexes, exhibit flexible and adjustable luminescence potentials and wavelengths as a result of introducing substituents on their cyclometalated ligands or changing their coordination ligand, they are mainly applied in organic solutions and cannot be used as labels for multitarget bioassays. (3) The redox potential of traditional ECL luminophores/co-reactants is usually high (greater than -1.2 V or even -2 V vs Ag/AgCl). However, at such high cathode potentials, the dissolved oxygen in the electrolyte produces ECL, which causes background signals and reduces sensitivity [104-110].

Although developing ECL with good potential resolution in a limited potential window is very difficult [111,112], several methodologies for multicomponent analysis have been exploited and shown extremely high sensitivity and accuracy. Gao *et al.* [113] synthesized the cyclometalated Ir (III) complex $(\text{dfppy})_2\text{Ir}(\text{dcbpy})\text{PF}_6$ with high quantum yields and good solubility in aqueous solution. They combined this complex with $\text{Ru}(\text{bpy})_2(\text{mcbpy-O-Su-ester})(\text{PF}_6)_2$ in the presence of tripropylamine to acquire well-separated strong ECL emissions at +0.9 and +1.4 V vs Ag/AgCl and the large difference of the ECL peak potential (~ 0.5 V) at the gold electrode.

Song *et al.* [114] synthesized a new type of low-potential cathode luminophore, namely, *N,N*-bis-(3-dimethylaminopropyl)-3,4,9,10-per tetracarboxylic diimide (PDI), with $K_2S_2O_8$ as the co-reactant. This luminophore can produce ECL responses at -0.6 V (Figure 6C). In addition, in contrast to other single-emission emitters, the J-type PDI dimer formed by the excitation of PDI in the ECL reaction had double ECL emission with a wavelength peak of 717–718 nm at $-0.25/-0.26$ V, thus showing a unique built-in self-calibration capability for accurate quantitative and biological imaging analyses. In this study, PDI and luminol were used as the potential-resolved luminants to measure carcinoembryonic antigen and AFP simultaneously over the low potential range of -0.6 V to 0.6 V. In combination with the monomercapto-stabilized CdTe QDs (GSH stabilized-CdTe (GSH-CdTe QDs)) that are commonly used as ECL luminophores (-1.25 V), Liu *et al.* [115] introduced 2,3-dimercapto-succinic acid-stabilized CdTe (DMSA-CdTe) QDs into a multiplex ECL system as another signal probe with a relatively low emission potential (-0.89 V vs Ag/AgCl) (Figure 6D). Given the homogeneity of the two luminophores, DMSA- and GSH-CdTe QDs had similar luminescent mechanisms in an aqueous environment. The emissions of the two luminophores were assisted by H_2O_2 , the collective co-reactant that was self-produced *in situ*, thus forming a benign and simple nano-ECL multimarker detection system. Li *et al.* [16] realized potential-resolved ECL in the single anodic region by using CIS@ZnS NCs and $(Ru(bpy)_2(dcbpy))^{2+}$ as luminophores and N_2H_4 as the co-reactant in aqueous solution. In this system, CIS@ZnS NCs/ N_2H_4 emits at the ultralow potential of 0.30 V, whereas $Ru(bpy)_2(dcbpy)^{2+}/N_2H_4$ presented emission from 1.00 V to 1.40 V (Figure 6E). The large separation in onset potential led to a high resolution of 2.60 V that far exceeded the 1.50 V threshold for the total baseline separation. The good resolution of this strategy in the monodispersed and immune-sensing states (baseline separation, $R_s \geq 1.5$) proved its usefulness in dual-component assays for practical applications.

Anti-cross-talk Strategy in the Simultaneous Detection of Multiple Markers

In ECL multimarker analysis, the potential-resolved ECL emitter pairs that can avoid mutual interference between the co-reactants and RET between luminophores are very limited. A series of strategies have been reported to solve the cross-talk between luminescence systems. Moreover, some ECL platforms for the detection of multiple markers have been proposed to expand the application potential of multimarker detection.

Spatial-resolved System

The resonance transfer of energy between light-emitting systems can be reduced by separating these systems from each other by a certain distance in space. The distance between different ECL probes must exceed nanometers to eliminate interference between ECL probes on one electrode. Zhou *et al.* [116] introduced a patterned indium tin oxide (ITO) electrode with three spatially resolved regions (with the spacing of 1.5 mm) and combined the three latent tuberculosis infection (LTBI) marker antibodies IFN- γ -Ab1, TNF- α -Ab1, and IL-2-Ab1 on the three spatially resolved regions. By using luminol, carbon QDs, and CdS QDs as potential-resolved ECL probes and $K_2S_2O_8$ (0.1 M) and H_2O_2 (10 mM) as co-reactants, ECL emission peaks with the peak voltages of $+0.6$, -1.2 , and -1.8 V (vs Ag/AgCl) were obtained, thus achieving the simultaneous detection of the three types of LTBI markers (Figure 7A). In accordance with the same principle, Feng *et al.* [117] established a novel double-working electrode ECL aptamer sensor array on a self-made SPCE (Figure 7B). The SPCE substrate was composed of two carbon working electrodes (WE1 and WE2). The aptamer sensor array not only had multiple detection functions, it also avoided the cross-talk and cross-reaction between light-emitting systems. On the electrode surface, the complementary DNA sequence (MG cDNA or CPA cDNA) fixed on the luminophore (CdS QDs (-1.15) or luminol-Au($+0.6$ V)) hybrids with the aptamer modified by the quencher Cy5 (quencher for CdS QD) or chlorogenic acid (CA, quencher of L-AuNP) formed two double-stranded structures on WE1 and WE2. In the presence of the target malachite green (MG) and CAP, the combination of MG and CAP with the aptamer resulted in the cleavage of the corresponding double-stranded structure, making Cy5 and CA separate from SPCE such that the ECL intensities of the cathode and anode increased simultaneously. This strategy could be used to detect MG and CAP with linear ranges of 0.1 – 100 and 0.2 – 150 nM, respectively, and detection limits of 0.03 and 0.07 nM, respectively.

Concentration-controlled Measures

In addition to eliminating cross-talk between light-emitting systems by means of spatial resolution, the influence of cross-reactions can be avoided by controlling the amount of luminophores or co-reactants that can cause cross-talk. Guo *et al.* [118] proposed the combination of Ru-NH $_2$ and AuNPs/g-C $_3$ N $_4$ as two potential-resolving luminous bodies and DBAE and $K_2S_2O_8$ as the co-reactants with two strong and stable ECL emissions at 1.25 and -1.3 V, respectively (Figure 7C). However, during the positive potential scanning, DBAE was oxidized and

deprotonated on the electrode into the strongly reduced intermediate DBAE⁻; which not only reduced the electrode oxidation product Ru³⁺ to produce ECL emission but also reacted with the reduction product of K₂S₂O₈, the co-reactant of g-C₃N₄. Therefore, the concentration of K₂S₂O₈ interfered with the production of the ECL signal by the luminophore Ru-NH₂ and the co-reactant DBAE. To reduce the system error, Guo *et al.* added excess DBAE such that the consumption of DBAE by K₂S₂O₈ was negligible, thereby eliminating the cross-reactions between the co-reactants of the dual luminescence system. Additionally, Han *et al.* [119] used Ru(bpy)₃²⁺ and luminol as the cathode and anode ECL probes on a single electrode to measure two antigens on the cell surface (Figure 7D). Although the potential-resolved

ECL based on the luminol/Ru(bpy)₃²⁺ system is feasible in principle, luminol cross-reacts with S₂O₈²⁻, which is the co-reactant of Ru(bpy)₃²⁺, and produces luminescence at the same potential as Ru(bpy)₃²⁺. The overlapping of the two luminescence peaks resulted in the nonlinear relationship between the logarithmic value of the concentration of the luminescent probe and the intensity of the lighting signal. To overcome the above problem, Guo *et al.* introduced high concentrations of the water-soluble luminol, which caused the self-quenching of its reaction with S₂O₈²⁻ under negative potential. This approach thereby greatly reduced the signal cross-talk generated by the cross-reaction of luminol and Ru(bpy)₃²⁺ with their mutual co-reactants at each other's luminous potential.

Table 6. Summary of partial reports on potential-resolved multiplex analysis by ECL technology. Unavailable measurements are represented by "-"

	ECL probe & onset potential	Target	LOD	Linear range	Ref.
Bilateral anodic-and-cathodic-potential luminescence					
1	CdTe@CdS QDs; -1.12 V Luminol; +0.6 V	AFP CEA	1.0 × 10 ⁻¹⁶ g/mL 1.0 × 10 ⁻¹⁶ g/mL	2.5 × 10 ⁻¹⁶ -2.0 × 10 ⁻¹¹ g/mL 2.5 × 10 ⁻¹⁶ -2.0 × 10 ⁻¹¹ g/mL	[121]
2	CdS QDs; -1.15 V L-AuNPs; +0.6 V	MG CAP	3.0 × 10 ⁻¹¹ M 7.0 × 10 ⁻¹¹ M	1.0 × 10 ⁻¹⁰ -1.0 × 10 ⁻⁷ M 2.0 × 10 ⁻¹⁰ -1.5 × 10 ⁻⁷ M	[117]
3	Ru-NH ₂ ; 1.25 V AuNPs/g-C ₃ N ₄ ; -1.3 V	CA125 SCCA	4.0 × 10 ⁻⁴ U/mL 3.3 × 10 ⁻¹³ g/mL	0.001-100 U/mL 1.0 × 10 ⁻¹² -1.0 × 10 ⁻⁷ g/mL	[124]
4	AuNPs/luminol; +0.6 V Ru(bpy) ₃ ²⁺ ; -1.0V	CEA AFP	- -	3.3 × 10 ⁻⁹ -1.6 × 10 ⁻⁸ g 2.0 × 10 ⁻¹⁰ -1.1 × 10 ⁻⁹ g	[125]
5	Luminol; 0.6 V g-C ₃ N ₄ ; -1.5 V	Acetamiprid Malathion	1.5 × 10 ⁻¹⁴ M 1.8 × 10 ⁻¹⁴ M	1.0 × 10 ⁻¹⁰ -1.0 × 10 ⁻¹³ M 1.0 × 10 ⁻¹⁰ -1.0 × 10 ⁻¹³ M	[101]
6	DMSA-CdTe QDs; -0.89 V TiO ₂ -GSH-CdTe QDs; -1.25 V	AFP AFP-L3	1.0 × 10 ⁻¹² g/mL 3.2 × 10 ⁻¹² g/mL	1.0 × 10 ⁻¹² -2.0 × 10 ⁻⁸ g/mL 3.2 × 10 ⁻¹² -3.2 × 10 ⁻⁸ g/mL	[115]
7	g-C ₃ N ₄ @AuNPs; -1.4 V Ru-MOF; +1.5 V	miRNA-141 miRNA-21	3.0 × 10 ⁻¹⁶ M 3.0 × 10 ⁻¹⁶ M	1.0 × 10 ⁻¹⁵ -1.0 × 10 ⁻¹¹ M 1.0 × 10 ⁻¹⁵ -1.0 × 10 ⁻¹¹ M	[126]
8	AuPNs/PDI; -0.6 V AuPNs/luminol; +0.6 V	CEA AFP	7.3 × 10 ⁻¹⁴ g/mL 5.6 × 10 ⁻¹⁴ g/mL	1.0 × 10 ⁻¹³ g/mL-1.0 × 10 ⁻⁹ g/mL 1.0 × 10 ⁻¹³ g/mL-1.0 × 10 ⁻⁹ g/mL	[114]
9	Luminol; +0.6 V Carbon QDs; -1.8 V CdS QDs; -1.2 V	IFN-γ TNF-α IL-2	1.6 × 10 ⁻¹² g/mL 1.6 × 10 ⁻¹² g/mL 1.6 × 10 ⁻¹² g/mL	1.6 × 10 ⁻¹² -2.0 × 10 ⁻¹⁰ g/mL 1.6 × 10 ⁻¹² -2.0 × 10 ⁻¹⁰ g/mL 1.6 × 10 ⁻¹² -2.0 × 10 ⁻¹⁰ g/mL	[116]
10	Au @ BSA MSs-luminol; 0.32 V TZZ; -1.8 V	2,6-Sialylated glycans 2,3-Sialylated glycans	3.3 × 10 ⁻¹⁵ g/mL 2.1 × 10 ⁻¹⁵ g/mL	1.0 × 10 ⁻¹⁴ -1.0 × 10 ⁻² g/mL 1.0 × 10 ⁻¹⁴ -1.0 × 10 ⁻² g/mL	[127]
11	Ru(bpy) ₃ ²⁺ ; +1.2 V Carbon nanodots; -1.2 V	AFP CA153 CA199 CEA	2.0 × 10 ⁻¹¹ g/mL 5.0 × 10 ⁻³ U/mL 6.0 × 10 ⁻³ U/mL 4.0 × 10 ⁻¹² g/mL	- - - -	[128]
12	Ru [phen] ₃ ²⁺ ; +1.2 V Concanavalin A-conjugated AuNP-modified graphite-C ₃ N ₄ ; -1.6 V	MCF-7 cancer cells N-glycan expression	15 -	1.0 × 10 ² -1.0 × 10 ⁶ cells/mL -	[129]
Unilateral low-potential luminescence					
	ECL probe and onset potential	Target	LOD	Linear range	Ref.
13	[dfppy] ₂ Ir(dcbpy)PF ₆ ; +1.4 V [Ru [bpy] ₂ [mcbpy-O-Su-ester] [PF ₆] ₂ ; +0.9 V	MMP-2 MMP-7	5.0 × 10 ⁻⁹ g/mL 1.0 × 10 ⁻¹¹ g/mL	1.0 × 10 ⁻⁸ -3.0 × 10 ⁻⁷ g/mL 5.0 × 10 ⁻¹¹ -1.0 × 10 ⁻⁹ g/mL	[7]
14	CIS@ZnS NCS; 0.10 V [Ru [bpy] ₂ [dcbpy]] ²⁺ ; 1.06 V	PSA CA125	- -	- -	[130]
Other miscellaneous potential-resolved luminescence					
	ECL probe and onset potential	Target	LOD	Linear range	Ref.
15	CdS nanowires; - RuSi@ Ru(bpy) ₃ ²⁺ NPs; -	Myo cTnl	2.0 × 10 ⁻¹³ g/mL 5.0 × 10 ⁻¹³ g/mL	5.0 × 10 ⁻¹³ -5.0 × 10 ⁻⁷ g/mL 1.0 × 10 ⁻¹² -1.0 × 10 ⁻⁷ g/mL	[131]
16	Luminol-AuNPs; - ABEL-AuNPs; -	Adenosine Thrombin	2.2 × 10 ⁻¹² M 1.2 × 10 ⁻¹⁴ M	5.0 × 10 ⁻¹² -5.0 × 10 ⁻⁹ M 5.0 × 10 ⁻¹⁴ -5.0 × 10 ⁻¹⁰ M	[132]
17	Au@luminol; CdS QDs;	MCF-7 cells Mannose EGFR	20 - -	1.0 × 10 ² -1.0 × 10 ⁶ cells/mL 1.0 × 10 ⁻¹³ -1.0 × 10 ⁻¹² M 1.0 × 10 ⁻¹⁰ -1.0 × 10 ⁻⁹ g/mL	[133]

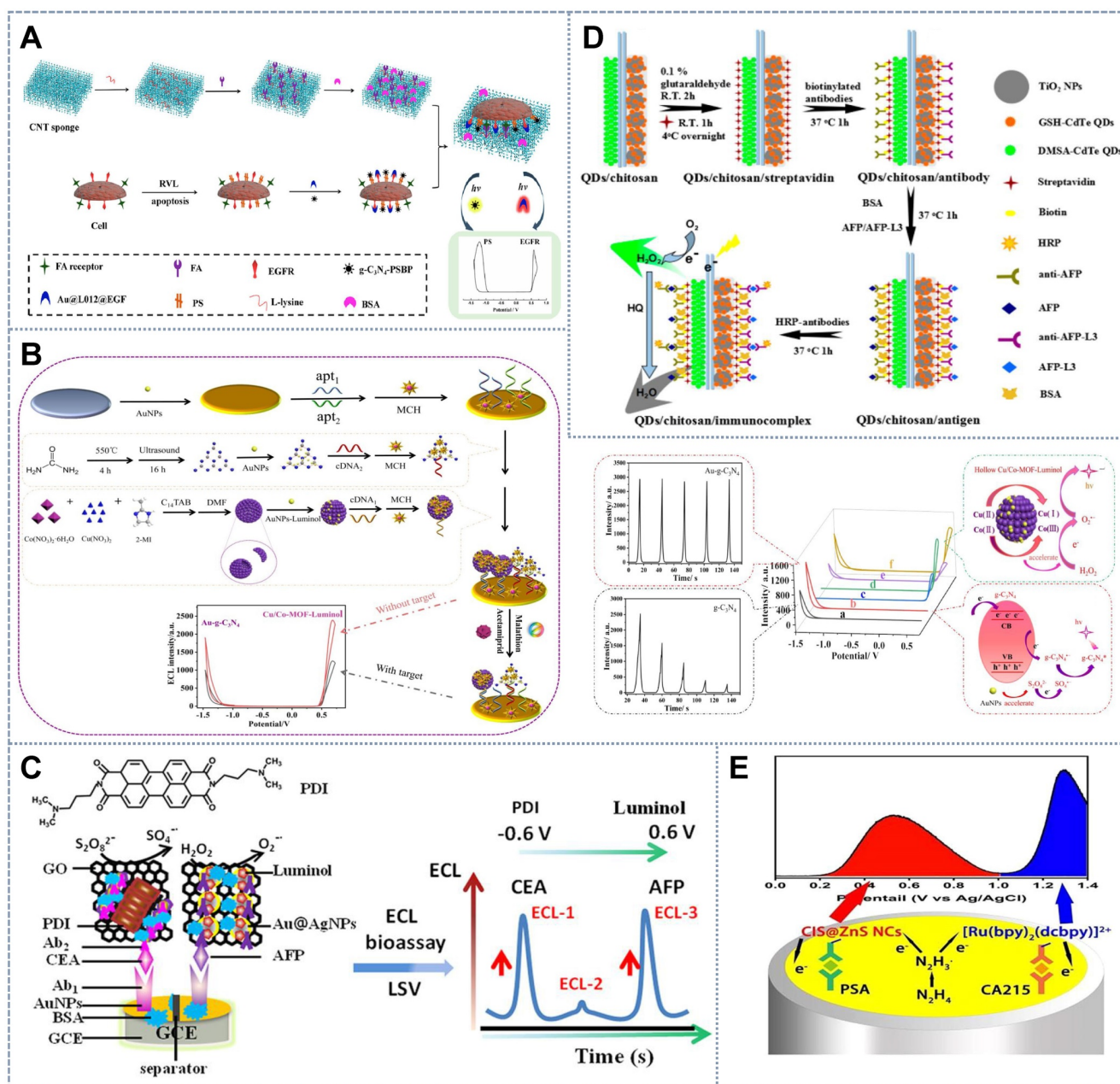


Figure 6. Schematic of sensors for simultaneous multimarker detection based on bilateral anodic-and-cathodic-potential luminescence with (A) L012 and g-C₃N₄ as the luminophore pairs for the *in situ* detection of apoptosis factors. Adapted with permission from [26], copyright 2019 American Chemical Society. (B) Luminol and g-C₃N₄ as the signal probe. Adapted with permission from [101], copyright 2021 Elsevier B.V. Biosensors based on unilateral low-potential luminescence with (C) the low-potential cathode luminophore PDI and co-reactant K₂S₂O₈. Adapted with permission from [114], copyright 2019 American Chemical Society; (D) homogenous luminophores GSH-CdTe QDs and DMSA-CdTe QDs sharing the co-reactant H₂O₂. Adapted with permission from [115], copyright 2021 Elsevier B.V.; and (E) CIS@ZnS NCs emitting at the ultralow potential of 0.30 V and [Ru(bpy)₂(dcbpy)]²⁺ as luminophores. Adapted with permission from [16], copyright 2021 Elsevier B.V.

Real-time and On-spot Detection

On-spot detection is a popular research direction for biosensors. The development of real-time detection and easy-to-carry biosensors is a prerequisite for the development of the Internet-of-Things [120,121]. Microfluidic paper-based analytical devices (μ -PADs) and paper-based analytical devices are considered excellent equipment for point-of-care testing because of their low cost, ease of use, ability to save reagents, portability, and disposability. These

paper-based devices can freely adjust the fluid flow driven by the inherent capillary force after sample loading and immune response, thus allowing simultaneous parallel and multiple measurements. Wang *et al.* [122] introduced the potential-resolved multimarker detection mode into μ -PAD devices for the first time (Figure 8A). Ru(bpy)₃²⁺ (+1.2 V) and carbon nanodots (CND) (-1.2 V) fixed on a screen-printed carbon working electrode were used as ECL probes. The two double-probe-labeled working electrodes enabled the simultaneous detection of four

tumor markers. In this system, the traditional electrochemical workstation was replaced with a battery, and the output voltage of the battery was precisely controlled by a low-cost and simple voltage controller. In accordance with the detection mode of potential discrimination, multiple immunoassays can be performed in one work area by only adjusting the direction of the positive and negative connections between the paper detection platform and the power supply device. This battery-based microfluidic ECL immunosensor provides a new strategy for high-throughput, low-cost, sensitive, and automated multiple immunoassays and instant diagnosis. On the basis of this research, Li *et al.* [123] designed a self-assembled toggle switch that can automatically switch the positive and negative potentials of the working electrode (Figure 8B). By using Ru(bpy)₃²⁺-conjugated silica NPs as the anode ECL label (+1.20 V), carbon nanocrystals deposited silica nanoparticles (CNCs@Si NPs) as the cathode ECL label (-1.20 V), and replacing the traditional three-electrode, ceramic or paper-based devices by transparent, low-cost ITO based two-electrode system, a low-cost, portable and battery rechargeable constant voltage ECL multiple immunosensor was developed with an output voltage of 1.20 V, which was employed to detect CA 153 and CA 199 with detection limits of 1.3×10^{-4} U ml⁻¹ and

2.3×10^{-4} U ml⁻¹, respectively. The constant potential ECL system based on rechargeable batteries showed good stability and repeatability. Furthermore, cheap and portable multimarker real-time detection systems can be obtained by replacing the expensive electrochemical workstations in some ECL systems with rechargeable batteries.

Potential-resolved Multicolor ECL

As discussed above, the potential-resolved strategy could greatly simplify operation and reduce the analytical time of ECL detecting systems because it does not require a filter or beam splitter, unlike other resolved strategies, such as the spatial-resolved strategy or the spectrum-resolved strategy. Nevertheless, with the expansion of the requirements for the number of output signals, the application of the potential resolved strategy alone can no longer meet demands because of the following restrictions: (1) When the electrode potential exceeds the corresponding threshold value, the ECL of each luminophore is persistently generated [22]. (2) The pairing of ECL probe pairs with indistinct onset-potential differences results in poorly resolved emission [134]. One general solution to this current challenge is to combine a potential-resolved strategy with spectrum-resolved strategy [135,136]. The

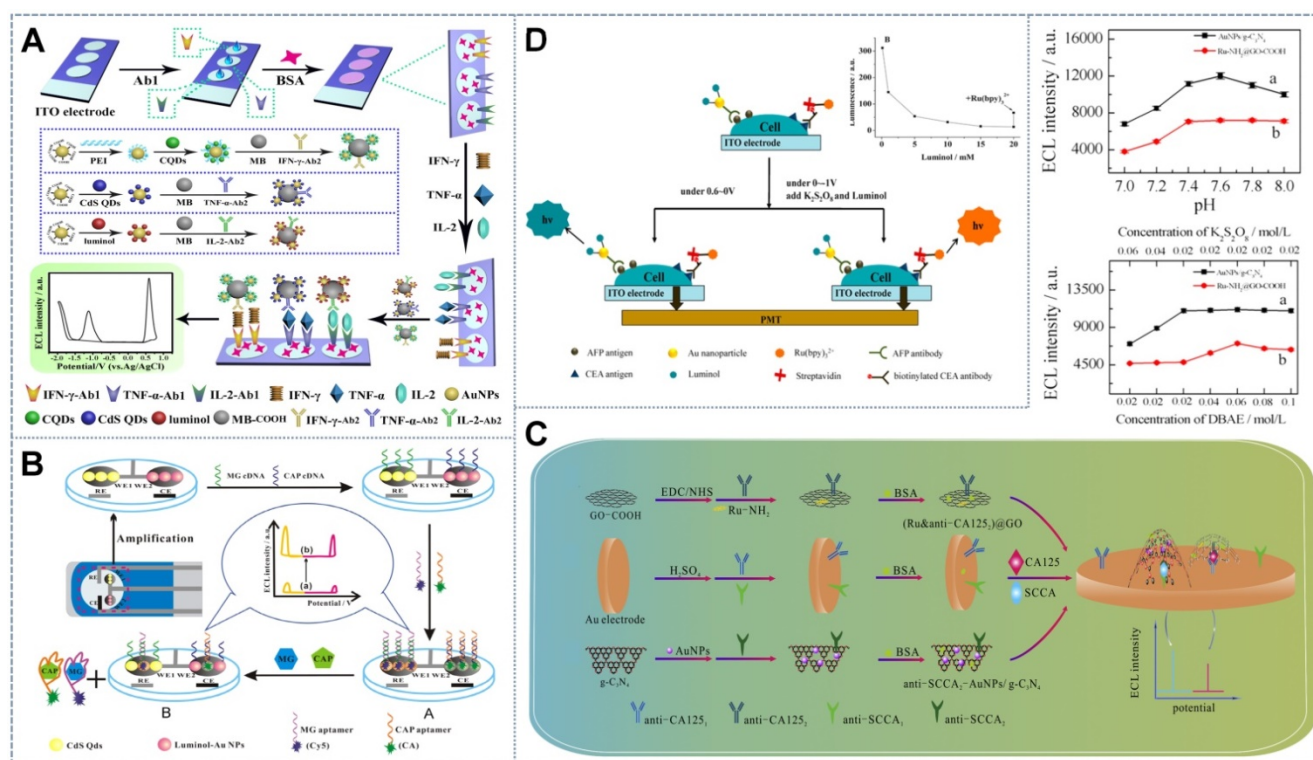


Figure 7. Schematic of anti-cross-talk multidetection sensors based on spatial-resolved strategy with (A) an ITO electrode with three spatially resolved regions for the detection of three biomarkers. Adapted with permission from [116], copyright 2017 American Chemical Society; (B) excessive DBAE. Adapted with permission from [117], copyright 2017 Elsevier B.V.; (C) a novel double working electrode aptamer sensor array on a SPCE. Adapted with permission from [118], copyright 2015 Elsevier B.V.; and the concentration-controlled strategy with (D) the high concentration of luminol. Adapted with permission from [119], copyright 2014 American Chemical Society.

spectrum-resolved technique, in contrast to the potential-resolved strategy, distinguishes the signal based on the varied emission wavelengths between emitters [14]. Therefore, when the peak potential of the two emitters is relatively close to causing the signal peak to overlap, the luminous intensity at distinct wavelengths may be utilized to identify the analyte [22]. Furthermore, the luminous wavelength of the luminophor is mostly unaffected by the potential or other substances in the system [137]. Consequently, the combination of potential resolution with spectral resolution can broaden the potential sweep and enable the simultaneous detection of multiple markers. Following the development of monochromatic electrochemiluminophores of different wavebands [138] and a CCD-based ECL spectrum analyzer [139], the key obstacles in spectrum-based ECL could be resolved, which makes it qualified for the potential-resolved and color-selective ECL models. This strategy is also known as “potential-resolved multicolor electrochemiluminescence (PRMCECL)”, specifically, multicolor ECL emissions under different potentials during an electrochemical scan [140]. The application of the PRMCECL strategy in ratiometric [141,142] and multiplex ECL assays [134] has attracted substantial attention given that it either provides additional signal information for self-calibration or enables the concurrent detection of multiple analytes. In addition, on the basis of its sufficiently powerful optical signal output, it can be utilized to construct and optimize visualized ECL sensors, which have now become popular for their direct and intuitive data readout pattern that is visible to the naked eye. Given the human eye’s low sensitivity to the resolution of monochromatic intensity, which leads to low detection sensitivity and the formation of erroneous conclusions, many visual signals are now only employed for quantitative or semiquantitative analysis [143]. The luminescence color of luminophor pairs possessing potential-resolved and wavelength-resolved properties can be used to determine analyte concentration quantitatively, which is critical to the development of multichannel bioassays and to reduce detection costs [14,144,145]. In accordance with different luminescence and reaction pathways, PRMCECL can be divided into concomitant metal complexes and single luminescent clusters, of which concomitant metal complexes have two luminous pathways: co-reactant multicolor ECL and annihilation multicolor ECL [116,145-148].

Concomitant Metal Complexes

Metal coordination complexes have attracted tremendous research attention and have been

successfully developed in the PRMCECL system due to their remarkable features, such as rapid response time; wide dynamic range; low sample consumption; high on-board stability; excellent precision; and, most importantly, zero-background sensitivity [135, 149-153]. When the ECL signal output must be clearly spectrally resolved to perform multiple assays, cyclometalated Ir complexes with emission maxima spanning the entire visible spectrum are used [154-159], thus opening up new possibilities for color-tunable light-emitting devices and simultaneous multianalyte detection based on multiple spectrally distinct ECL species [135,160-163].

The PRMCECL strategy can be divided into three categories in accordance with the choice and synthesis of the concomitant metal complex and the construction of the ECL system. The first type of multicolor ECL is a mixture consisting of Ru(II) and Ir(III) complexes. For example, given that the luminescence of Ru(bpy)₃²⁺ and its derivative complexes is characterized by a broad spectral line width (FWHM of 60–80 nm) [134,164], long radiative decay lifetime (typically microseconds) [165], low photoluminescence (PL) quantum yield (PLQY, ~ 4.2% for Ru(bpy)₃²⁺), and difficult multicolor detection, Guo *et al.* [134] expanded the spectral coverage of the concomitant metal complexes by synthesizing several Ru and Ir complexes with distinguishable ECL emission wavelengths that ranged from 491 nm to 636 nm (Figure 9A). The ECL performance of the mixtures was investigated by using multiple ECL readout modes (intensity, spectrum, and imaging measurements). A spectral peak separation of up to 145 nm was found between the cyan-ECL-generating species Ir(dFCF₃ppy)₂(dtbbpy)⁺ and the red-ECL-generating species Ru(bpy)₂(dvbpy)²⁺. Therefore, the mixed electrochemiluminescent system achieved spectrally resolved ECL generation. Potential-resolved ECL emissions were obtained by using Ir(ppy)₃, a green-ECL luminophore with self-annihilating ECL behavior at high potentials, for the quenching of (Ir(ppy)₃)^{*} by TPrA⁺ with either Ru(bpy)₂(dvbpy)²⁺ or Ir(dFCF₃ppy)₂(dtbbpy)⁺. A multiplex immunoassay (MIA) free of spatial spotting antibodies on plates or substrates was ultimately devised by combining luminophore-loaded polymer beads with the homogeneous sandwich immunoreaction method. The simultaneous recognition of three antigens through the use of the potential and spectrum dual-resolved ECL as the readout signal illustrated the vast potential of this approach for multiplex ECL detection. The second type of multicolor ECL is from multimetal (e.g., Ru²⁺ and Ir³⁺) centers within a single molecule. Previously reported work usually used Ir

and Ru complexes as ECL emitters and regulated the applied potential to achieve spectral resolution [135]. However, this strategy relies on intermolecular reactions between two emitters and can be easily interfered with by other substances in the system because of steric hindrance and energy loss [167]. This problem can be solved by combining two luminophores into one molecule and relying on intramolecular interactions. For example, Peng *et al.* creatively designed and synthesized heterodinuclear (bpy)₂Ru(bpy)(CH₂)_n(bpy)Ir(df-ppy)₂]³⁺ (n = 10, 12, 14) complexes that combined Ir and Ru in a single molecule. The color of the light can be changed by regulating the applied potential in accordance with the intramolecular interactions between the Ir and Ru moieties. When the scan potential ranged from 0.55 V to 0.95 V, the ECL intensity at 543 nm from the Ir moiety and that at 618 nm from the Ru moiety showed good linear calibration curves. When the scanning voltage ranged from 1.0 V to 1.6 V, the emission from the Ru moiety increased rapidly, whereas the Ir moiety had little or no emission due to the RET between the Ir and Ru moieties. This strategy can also help find new ECL luminophores. Sun *et al.* combined luminol with the classical dyes 7-(diethylamino) coumarin-3-carboxylic acid (CO) and 3-(4-amino-1,8-naphthalimido) propanoic acid (NA). The dyes were ECL inactive originally, but because of the energy resonance transfer between luminol and the dyes, the LU-CO and LU-NA complexes exhibited emission under the potential of 0.5 V at 481 and 540 nm, respectively [168]. The third type of multicolor ECL originated from light-emitting devices, which combine solid-state ECL materials (metal complexes) with organic light-emitting diodes (e.g., small organic molecules and polymers). Sandwich-structured organic light-emitting diodes (OLEDs) and solid-state electrochemiluminescence devices (SECLDs) that usually use Ru tribipyridine as the luminescent molecule have received considerable attention. However, their operation mechanisms have many differences, such as carrier injection and hole and electron mobility. De Cola *et al.* designed a new light-emitting device that combined OLEDs and SECLDs together to obtain some insight into equipment characteristics, such as electronic injection and recombination, and seek new ways for instrument optimization. In their work, 3% wt (Ru(bpy)₂(dimbp))(PF₆)₂ in pyridine solution, aluminum tris-(8-hydroxyquinoline)(Alq₃), and *N,N'*-diphenyl-benzidine were loaded on an ITO in sequence. The ECL emission centered at 625 nm was acquired under reverse bias (-10 V). The color of the light changed from yellow to green to white over time under forward bias (+9V) [169].

ECL emission principles are often categorized into two general pathways: annihilation and co-reaction. Both pathways play an important role in PRMCECL. The first co-reactant multicolor ECL was reported by Richter *et al.* [135], who utilized the combinations of (Ru(bpy)₃)²⁺ (I_{max} = 620 nm) and either fac-Ir(ppy)₃ (I_{max} = 517 nm) or (Ir(df-ppy)₂(pic)) (I_{max} = 498 nm) with TPA as the oxidative-reductive co-reactant that generated simultaneous ECL from the two luminophores (albeit with considerable overlap between emission bands) at the single applied potential of 0.8 V. Doeven *et al.* [170] demonstrated that by scanning or stepping from low to high electrode potentials, the mixtures of electrochemiluminophores may also be identified selectively on the basis of their unique redox energies. For example, in the presence of a green-emitting (Ir(df-ppy)₂(BPS))⁻ complex, a red-emitting (Ru(bpy)₂(L))²⁺ complex was stimulated preferentially at a low electrode potential (1.05 V vs. Fc^{0/+}), and simultaneous ECL from the two complexes was detected at a high electrode potential (1.30 V vs. Fc^{0/+}), thus allowing the total emission color to be adjusted from red to yellow-green. Similarly, Schmittle *et al.* [171] demonstrated that the ratio of emissive transitions within a non-Kekulé e-structured trinuclear Ir(III)-Ru(II)-Ir(III) species was dependent on the applied potential. The wavelength of maximum ECL intensity could be tuned between 649 and 611 nm as the anodic scan range was increased. However, these findings cannot realize complete and reversible switching between the emissions from two distinct ECL luminophores due to the difficulty in switching off the low-potential electrochemiluminophore at potentials where the high-potential luminophore is excited. Such a situation may induce the unwanted interference of the emissions of two luminophores in multiplex ECL-based assays. Therefore, by exploiting the switch-off mechanism of Ir(ppy)₃ at high overpotentials likely through the oxidative quenching of the excited (Ir(ppy)₃)^{*} state, Doeven *et al.* [170] selectively elicited green ECL from Ir(ppy)₃ at low potentials and either red or blue ECL from (Ru(bpy)₂(L))²⁺ or Ir(df-ppy)₃ at high potentials. Although two-component mixed ECL systems have been extensively explored, their application in high-throughput testing remains limited. As a result, a system with additional luminators and resolved colors should be developed. However, the development of a three-color ECL system with the concomitant metal complex is hampered by the broad spectral distributions and significant spectral overlaps (i.e., 26% of the integrated peak area of Ru(bpy)₃²⁺ (max = 620) and fac-Ir(ppy)₃ (max = 520 nm)) of the conventional Ru- and/or Ir-complexes. To solve this problem, Doeven

et al. [172] modified the ligand structure to control the border orbital energies, which influence the complexes' spectroscopic and electrochemical characteristics. Specifically, they created a deep red emitter $[(Ru(bpy)_2(dm-bpy-dc)]^{2+}$, $\lambda_{max} = 685$ nm] by adding two electron-withdrawing methyl ester groups on one of the $(Ru(bpy)_3)^{2+}$ bpy ligands, thus producing a bathochromic shift in emission while preserving a favorable oxidation potential for ECL [173]. Similarly, the addition of fluorine groups to the phenyl rings of $Ir(ppy)_3$ caused a large hypsochromic shift by stabilizing the HOMO level of the mixed metal-ligand, resulting in a suitable blue emitter $(Ir(df-ppy)_3)$, $\lambda_{max} = 495$ nm [170]. A compound containing a triazolopyridinato ligand $(Ir(df-ppy)_2 [ptp])$, $\lambda_{max} = 463$ and 492 nm, which further

blue-shifted the emission and gave a three-fold boost in ECL intensity, was also created [174]. With these changes, spectrally resolved red and blue emitters (overlapping in the integrated peak area of just 5%) were obtained. In addition, a third concomitant electrochemiluminophore green-emitter $(Ir(ppy)_3)$ was used to extend the system for three-channel detection by taking advantage of the different potentials required for electrochemical excitation [122,160,161] and the recently discovered selective ECL quenching of the co-reactant $Ir(ppy)_3$ at high overpotentials [170]. Then, by employing separate applied potentials, the first multicolor ECL system with three effectively resolved emitters was demonstrated in combination with the intrinsic color selectivity of a standard digital camera.

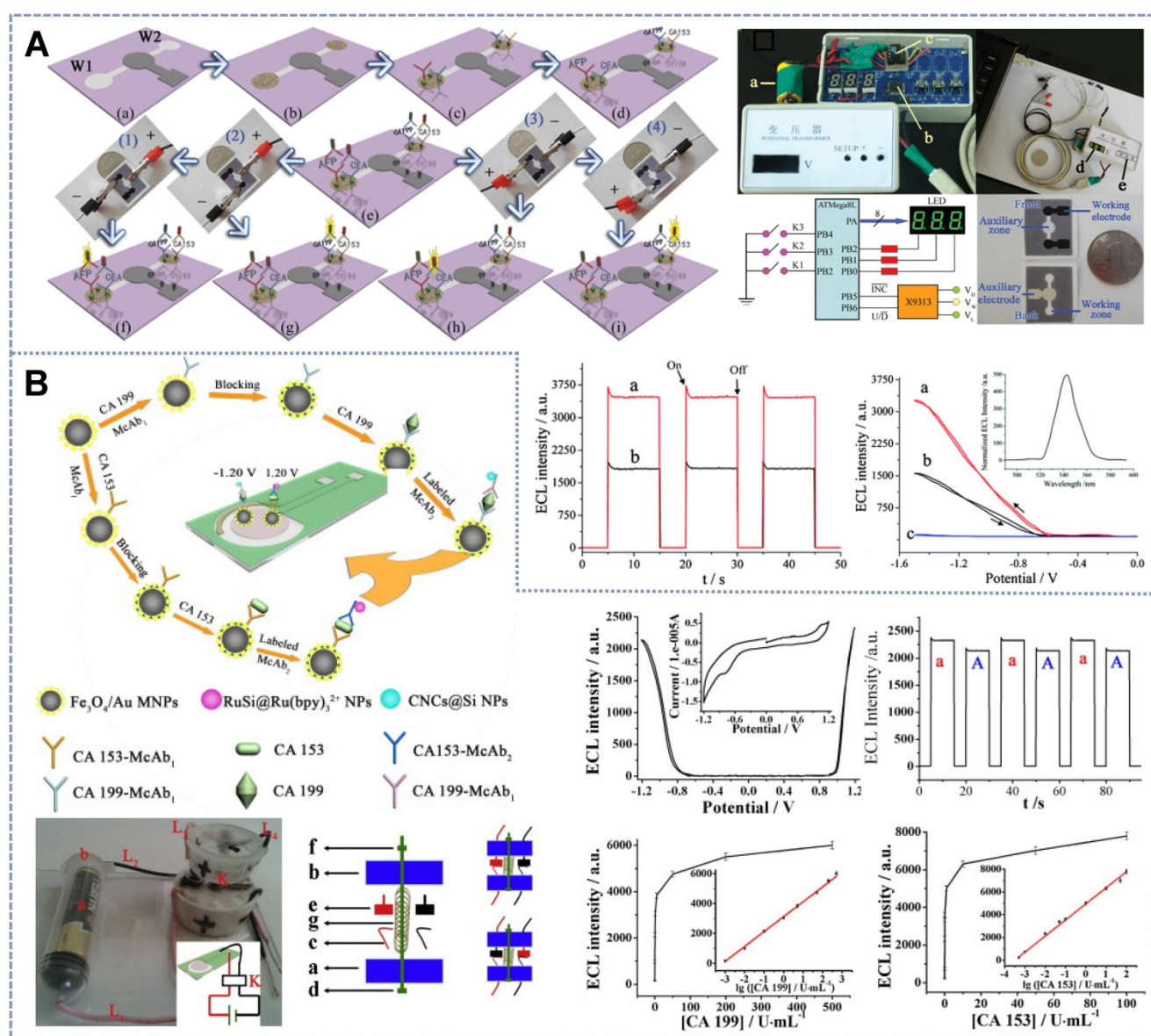


Figure 8. Schematic of biosensors with real-time and on-spot detection based on (A) a battery-based microfluidic paper. Adapted with permission from [122], copyright 2012 Royal Chemistry Society. (B) Automatically toggled switch. Adapted with permission from [123], copyright 2013 Elsevier B.V.

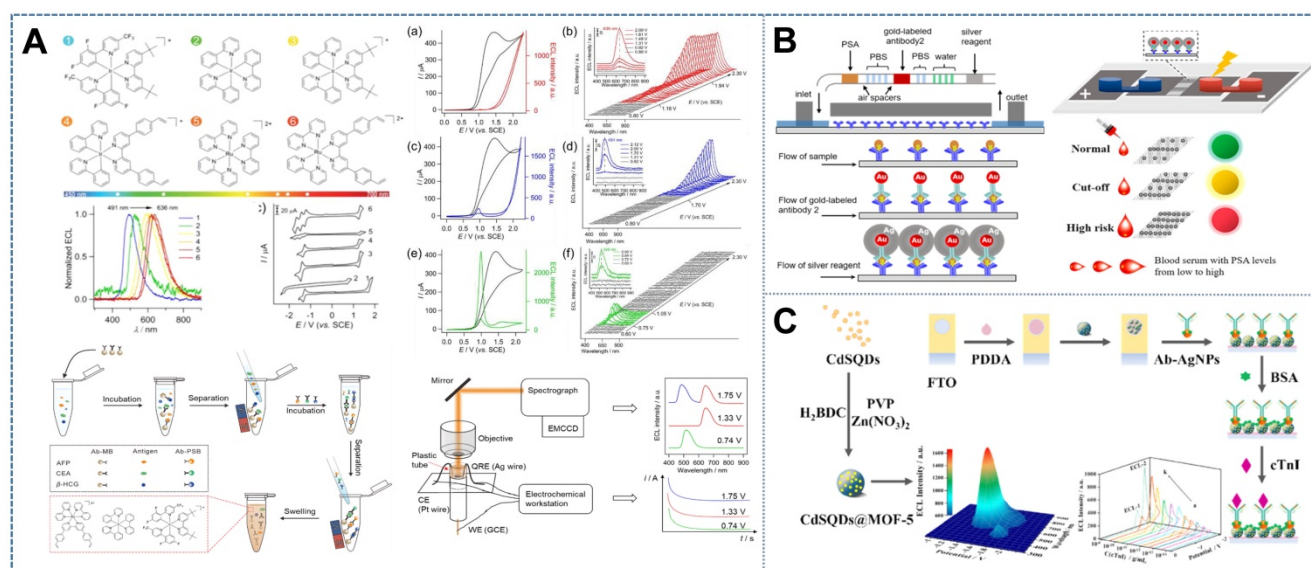


Figure 9. Schematic of the application of the PRMCECL strategy in (A) MIA by using several self-synthesized concomitant metal complexes with expanded spectral coverage. Adapted with permission from [134], copyright 2018 American Chemical Society. (B) Immunosensor visualization by regulating the interfacial potential ($\Delta\phi$) at the poles of BPE. Adapted with permission from [183], copyright 2017 American Chemical Society. (C) Ratiometric biosensor based on the PRMCECL nanoluminophore CdS QDs@MOF-5. Adapted with permission from [141], copyright 2020 American Chemical Society.

Another important concept is the annihilation route, in which oxidized and reduced species are produced at two separate electrode potentials and then comproportionated to produce an emissive excited state to provide an alternative to multicolor ECL. The mixed annihilation ECL of metal chelates containing more than one organic compound or a transition-metal chelate with a nonemissive organic compound [175] to generate the relative intensity of multiple luminophores (and thus overall emission color) that can be controlled initially by selecting the electrochemical and spectroscopic properties of the complexes, as well as the applied electrochemical potentials, was explored. The factors controlling the ECL emission color in mixed annihilation ECL are (1) the relative concentrations of two complexes [176-178]; (2) the relative ECL quantum yields; and (3) the efficiency of various energy transfer pathways [179], such as RET or electron transfer/exchange, among the numerous oxidized, reduced, ground, and/or excited states of the complexes that are probably determined by the numerous closely spaced reductions and oxidations of the mixed system. Kerr *et al.* [175] created the mixed annihilation ECL system of transition-metal complexes (combining $(\text{Ru}(\text{bpy})_3)^{2+}$ with a range of Ir(III) complexes), wherein the relative strength of the emissions could be adjusted by the applied voltage to alter the overall hue of the luminescence. This effect is due to the generation of distinct redox forms by the complexes that altered the energetics of the light-producing processes. In a subsequent study, Swanick *et al.* [180] investigated the ECL of a soft salt Ru(II)-Ir(II) complex [181], which

contained a $(\text{Ru}(\text{dtb-bpy})_3)^{2+}$ cation (dtb-bpy = 4,40-di-*t*-butyl-2,20-bipyridine) and two $(\text{Ir}(\text{ppy})_2(\text{CN})_2)^-$ anions (where ppy = 2-phenylpyridine), in solution. They reported that in contrast to the PL of the soft salt under nearly comparable conditions, ECL originated entirely from the Ru(II) complex (i.e., no emission from the Ir(III) complex). Swanick *et al.* [179] attributed their findings to the soft salt's ion pairing interactions, which assisted efficient quenching inside the mixed annihilation ECL system. Subsequently, Kerr *et al.* [182] reconciled these contradictory findings by investigating the concentration effects and energy transfer in mixed annihilation ECL. They also introduced a novel three-dimensional representation of the phenomenon (annihilation ECL intensity versus emission wavelength and the applied reduced potential), as well as a simple graphical depiction of the energetics of annihilation and co-reactant ECL systems, for the investigation of electron-transfer quenching pathways. They confirmed that the contradictory findings of previous studies can be largely attributed to differences in the relative concentrations of electrochemiluminophores; the relative ECL intensities of individual and mixed annihilation ECL reactions; and the efficiency of various energy transfer pathways, which are likely the result of a combination of several concomitant pathways that may include RET or electrification.

For the construction of PRMCECL biosensors, the bipolar electrode, a conductive material that promotes electrochemical reactions at its extremities under sufficient driving potential [183], has been widely utilized for multicolor visualization [184].

Selective ECL excitation is carried out by regulating the interfacial potential ($\Delta\phi_a$) at the poles of BPE on the premise of the potential resolution of the emission color of concomitant luminophores [185]. Wang *et al.* [183] devised the first PRMCECL device for biological analysis on the basis of closed BPE by utilizing a mixture of the red and green luminophores Ru(bpy)₃²⁺ and Ir(ppy)₃ with TPrA as the co-reactant (Figure 9B). A silver bridge with PSA-concentration-dependent properties was built in the gap between the BPEs to modulate resistance. By moderating the interfacial potential difference ($\Delta\phi_a$), the kinetics of Faradic reactions at the surface of the BPE would be altered, finally leading to a visible three-color change (green–yellow–red) at the anode. These eye-catching color changes could effectively reflect the cut-off values (4.0 and 10.0 ng/mL) of human PSA, thus demonstrating that the clinical use of the proposed PRMCECL biosensor is feasible and reliable. On this basis, Luo *et al.* achieved the rapid visual detection of the foodborne pathogen *Salmonella typhimurium* in a complex food matrix by taking advantage of the separate reservoir of the closed BPE system [186], in which the analytes were not in direct contact with the photoactive molecules in the complex reaction systems of the anode, thus efficiently avoiding mutual interference. The presence of *S. typhimurium* on the BPE cathode increased the resistance of the cathode. This effect induced the emission color of the Ir(ppy)₃ and Ru(bpy)₃²⁺ complexes to switch from dark-orange to yellow to forest-green. This phenomenon enabled the determination of *S. typhimurium* by the naked eye at the fairly low limit of detection of 10 CFU/mL in a 25 mL or 25 g sample within 0.5 h. Furthermore, in resistance-resolved BPE-ECL, cathode reactions, which alter the Faradaic current through BPE, could also be observed on the basis of the emission color of the anode. Wang *et al.* [145] introduced a special excitation potential combination containing Ru(bpy)₃²⁺ with the luminous peak voltage in between those of Ir(df-ppy)₂(pic), which enables the bidirectional change of the emission color (blue-green to red to blue-green) while either decreasing or increasing the Faradaic current. This array could simultaneously detect PSA, circulating microRNA-141, and the small molecular marker sarcosine with a single DC power supply. Therefore, the BPE-ECL device may greatly expand the construction strategies of PRMCECL biosensors, which have considerable potential applications in clinical diagnostics for the fast and intuitive judgment of multiple analytes.

Single Luminescent Clusters

In the last several years, PRMCECL nanoluminophores and QDs have emerged and shown

promising applications in sensitive and accurate bioassays, bioimaging, and multicolor-emitting devices.

Three types of potential-resolved multicolor ECL nanoluminophores have been reported. The first type is the ECL nanoluminophores without functionalization or hybridization. On a negative potential scan, Zhang *et al.* presented a dual-peak ECL system of carbon dots in ethanol with tetrabutyl ammonium bromide as the co-reactant; this system was used to identify iron ions via the internal standard method [187]. The second type is ECL nanoluminophores based on the hybridization of two nanomaterials. Ding *et al.* synthesized PbS nanocrystals capped with boron-dipyrromethene dye to produce highly efficient dual ECL emissions with tripropylamine as the co-reactant in organic solvents [188]. However, the multicolor ECL emissions generated in organic solvents were unsuitable for bioassays and biosensors. Later on, several kinds of nanoluminophores with the PRMCECL property in aqueous solutions were synthesized. They included the TiO₂-TCPP-ABEI (TCPP = 5,10,15,20-tetrakis-(4-carboxyphenyl)-porphyrin) nanoluminophore, nGO@TiO₂ nanoluminophore, and g-C₃N₄/ABEI nanoluminophore [189]. Furthermore, the applications of these nanoluminophores with the PRMCECL property in label-free ratiometric ECL immunosensors were explored on the basis of the intensity ratio of the potential-resolved ECL signals. However, given that analytes would contribute similar effects to the potential-resolved ECL signals, the use of ratio measurement strategies to obtain improved analytical performance or determine analytes was difficult. Du *et al.* developed a novel ECL nanoluminophore CdSQDs@MOF-5 by encapsulating CdSQDs into MOF-5. Two ECL peaks (ECL-1 and ECL-2) with different colors (with a wavelength of 685 and 475 nm) in the negative potential range (−1.4 and −1.8 V) were generated through the reaction of electroreduced CdSQDs^{•−} and MOF-5^{•−} with SO₄^{•−}. A label-free differential ECL immunosensor was successfully established to detect cTnI with syntropy change in the intensity of ECL-1 and ECL-2, and the synchronized interference that originated from two signals can be eliminated by the subtraction of one ECL signal from the other ECL signal in the potential-resolved ECL emissions [141] (Figure 9C). The third type is ECL-molecule functionalized nanoluminophores. Wang *et al.* synthesized ABEI-functionalized g-C₃N₄, which displayed two potential-resolved ECL peaks in the presence of K₂S₂O₈ and H₂O₂. On this basis, a metal ion-mediated potential-resolved ratiometric ECL bioassay for the detection of miR-133a was created [190]. Similarly,

Guo *et al.* successfully synthesized novel ABEL-functionalized QD ECL nanoluminophores with three completely potential-resolved dual-color ECL emissions and explored their usage in a label-free three potential ratiometric immunosensor for the detection of cTnI with the ECL-1/ECL-3 ratio as the self-correction reference. This work opened a new area in the research on the multicolor ECL of nanoluminophores, which is of great importance in the ECL field from fundamental studies to practical applications [142].

Recently, the interest in QD-based ECL systems has increased because of the large diversity, easy synthesis, extremely efficient and steady signal output, and adjustable photometric properties of QDs [191-193]. Li *et al.* [194], for the first time, successfully achieved the multicolor ECL of semiconductor nanocrystals tuned by the size effect by using QDs with a core-shell structure. This approach would provide guidance for the design and preparation of stable and strong multicolor ECL emitters for the simultaneous analysis of multiple components. Li *et al.* [194] systematically studied size-dependent colorful ECL emissions based on core-shell structured CdSe@ZnS QDs in aqueous solutions. The emission color of these QDs was tuned by selecting different sizes of cores. The CdSe@ZnS QDs with different sizes (2.5, 4.0, and 5.9 nm) presented novel colorful ECL emissions at approximately 525, 585, and 625 nm, which were identical to their PL. Similarly, Liu *et al.* [195] generated four sizes of water-dispersible CdS QDs capped with 3-mercaptopropionic acid. Particles emitting green, yellow, pink, and red ECL with positively shifted ECL onset potentials and continuously increasing ECL intensity were created by increasing the particle size of CdS QDs to 1.8, 2.7, 3.2, and 3.7 nm. However, all of the QDs used for ECL production showed significant surface trapping in their emission as evidenced by their shifted and trap-emitting ECL relative to their PL [196-199], resulting in a low PLQY [200-202] and/or multi-channel PL decay dynamics [203,204]. Comparative studies have shown that ECL is more vulnerable to surface traps on QD surfaces than PL, thus necessitating the creation of a distinct inorganic-organic interface to conceal traps [197,198]. Cao *et al.* [205] used the wide bandgap feature of ZnS shells to cover the surface traps on CdSe@CdS QDs, wherein intermediate CdS layers were built to relieve the considerable lattice strain between CdSe and ZnS. Under nonaqueous and aqueous conditions, the effectively synthesized CdSe/CdS/ZnS core/shell/shell QDs showed almost optimal PL characteristics, such as near-unity PLQY (>90%), narrow PL peak, and monoexponential PL decay dynamics. CdSe QDs

of various sizes (with average diameters of 5.9 nm (emitting at 549 nm), 6.6 nm (emitting at 592 nm), and 9.0 nm (emitting at 643 nm)) were chosen to obtain spectrally resolved ECL, and their emission wavelengths had to be adjusted to be 50 nm apart from each other. Such an adjustment relies on the regulation of the thickness of the CdS inner shell. The potential-dependent ECL spectra of the green-, yellow-, and red-emitting QDs produced brilliant and steady band-edge ECL that was not only narrow and symmetric but also easily visible and identifiable from one another by the naked eye. Overall, these qualities enabled the presentation of a potentially tunable system for spectrally resolved ECL, demonstrating that the overall ECL would vary its spectrally resolved pattern at various potentials. This approach not only enables detecting several different targets at the same time but also opens up new possibilities for developing multiplex assay.

Summary and Outlook

The potential-resolved strategy, as a basic methodology for ECL signal output, can guide the design and development of many sensors and has far-reaching academic and practical importance due to its low instrument requirement, short assay time, and good sample throughput. By recounting and discussing its applications in (a) ratiometric ECL sensors, (b) ECL sensors for the simultaneous detection of multiple markers, and (c) multicolor ECL sensors, the design criteria for the particular application mode of the three types of sensors in the potential-resolved strategy were gradually theorized and materialized to facilitate the discovery of new electrochemiluminophores with bespoke properties.

In general, for ratiometric ECL dual-potential biosensors, the most important problem of the traditional ECL-RET and co-reactant competing method is the lack of electrochemiluminescent system pairs for realizing the signal change along with the analyte. Therefore, some improvements in the traditional approach have been achieved, including the development of the dual-role energy transfer intermediate, universal enhancer or quencher, steric hindrance competition strategy, and competitive immunoassay. Studies related to these topics explained the design of sensors and the application of materials on the basis of chemical and electrochemical mechanisms, which are of great importance for guiding the application of theory. In addition, certain novel strategies, such as the enzyme-based ratiometric strategy and the single luminophore ratiometric system, have been found to augment the theoretical basis of the ratiometric ECL method. Furthermore, most previous studies on markers were based on

regulating the loaded ECL luminescer, which inevitably increases the complexity of system construction and chemical cross-talk. Therefore, these studies cleverly used the special properties of some co-reactants to control the generation and consumption of ECL co-reactants at different potentials via enzymatic reactions or special chemical reactions. Obtaining resolvable ECL signals within a narrowed potential is the key to increasing the number of the simultaneously detected substances of potentiometric multilabel ECL analysis systems. The main challenges are the limited number of ECL luminophores available and the ineffective control of electrochemical reactions by voltage. Although luminophores with different redox potentials can be easily synthesized, ECL is persistently generated as long as the potential exceeds the corresponding threshold value, which can be compensated for if each luminophore's emission can also be spectrally resolved. In this case, developing a signal probe with a low emission potential and narrow potential is another strategy. As previously stated, the potential-resolved multicolor ECL system in which the color of the combined ECL signal can be adjusted with various voltages can expand the valid potential scale to some extent and also enable the visualization of the detection results. Although these investigations have revealed new possibilities and breakthroughs for ECL analysis, comprehensive research remains to be conducted before the potential-resolved strategy could be extensively applied in the ECL bio-sensing field.

(1) Unique luminophores should be designed to increase data output in a narrow signal window to meet the requirements of clinical high-throughput testing. Several techniques that can provide theoretical possibilities exist: I. The ongoing development of new water-soluble low-potential emitters will improve the utilization of the potential window to achieve the simultaneous detection of biomarkers in the same batch. II. The use of electrochemiluminophores with narrow spectral distributions will enable the resolution of great numbers of emitters over a defined voltage range. III. Given that most ECL luminophores can react with multiple co-reactants to emit at different potentials, a single emitter within a multiple co-reactant system can be constructed for multiplex detection, in which markers can be labeled with multiple co-reactants to solve the problem of luminophore shortage. IV. Moreover, combining potential-resolved approaches with some spatial and/or spectral resolution will enable the performance of a considerably increased number of simultaneous assays within a relatively small detection zone.

(2) A large part of ECL reactions rely on H_2O_2 or dissolved oxygen as their co-reactants. However, some unresolved issues limit their clinical applications. These issues include the instability of H_2O_2 , which makes ensuring that the same concentration of H_2O_2 is added in every detection difficult. Moreover, the ultralow catalytic efficiency of dissolved O_2 for ECL necessitates the development of new methods to increase the amount of active co-reactants on the electrode surface. One strategy is to introduce novel ORR catalysts (such as biomimetic nanozymes and single-atom catalysts) that can generate a large number of ROS *in situ* by catalyzing dissolved oxygen in the solution. These catalysts are often macromolecules with carbon and nitrogen matrix backbones and metal active sites that confer them with the ability for self-enrichment and for binding biological macromolecules as tags through covalent modification, which can lead to the amplification of ECL signals.

(3) With the widespread application of the Internet-of-Things and increasing demand for point-of-care diagnostics, real-time, multiplex, and portable ratiometric ECL biosensors will be further developed and perfected against background of the in-depth exploration of the principle of potential discrimination technology. The early development of potential-resolved multiplex ECL suggests that the greatest benefit from these approaches lies in the development of low-cost portable analytical devices (for example, those based on paper microfluidics, rechargeable batteries, and/or supported by mobile phone technology), in which multiple, simultaneous, but still highly sensitive assays are desired.

Overall, the multisignal output ECL system based on a potential-resolved scheme is a promising and desirable strategy for the creation of diverse ECL sensors. Other preferable ECL materials, the deepened understanding of the design criteria for optimal electrochemical and photophysical properties, and the novel mechanisms of potential resolved ECL methodologies are all still being researched and developed.

Abbreviations

ECL: electrochemiluminescence; MIA: multiplex immunoassay; ECL-RET: electrochemiluminescence resonance energy transfer; $\text{Ru}(\text{bpy})_3^{2+}$: $\text{Tris}(2,2'$ -bipyridine) $\text{Ru}(\text{II})$; HRP: Horseradish peroxidase; PAMAM: Poly(amidoamine); CdS QDs: CdS quantum dots; Cy5: cyanine dye; PL: photoluminescence; CPB: CsPbBr_3 nanocrystals; Rh6G: rhodamine 6G; NPs: nanoparticles; NFs: nanoflowers; Cu_2O : cuprous oxide; FCA: ferrocenecarboxylic acid; HCNS: hollow graphitic carbon nitride nanospheres; ORR: oxygen

reduction reaction; PNK: polynucleotide kinase; ABEI: *N*-(aminobutyl)-*N*-(ethylisoluminol); DBAE: 2-(dibutylamino)ethanol; AuNPs: gold nanoparticles; MOF: metal-organic framework; Cu-TCPP(Zn): copper-based zinc porphyrinic; AFP: alpha fetoprotein; PFO: poly(9,9-dioctylfluorene); Hx: hypoxanthine; AChE: acetylcholinesterase; GSH: glutathione; ZEN: Zearalenone; NGQD: nitrogen-doped graphene quantum dots; TEA: triethanol-amine; CNTs: carbon nanotubes; cTnI: cardiac troponin I; SPCE: screen-printed carbon electrode; CAP: chloramphenicol; CdS NWs: CdS nanowires; L-AuNPs: luminol-gold nanoparticles; DDCE: dual-disk glassy carbon electrode; PSA: prostate specific antigen; CA: chlorogenic acid; g-C₃N₄: carbon nitride; Pdots: polymer dots; L012: 8-amino-5-chloro-7-phenylpyrido(3,4-d)pyridazine-1,4(2H,3H)-dione; Con A: concanavalin A; PDI: *N,N*-bis-(3-dimethylaminopropyl)-3,4,9,10-per tetracarboxylic diimide; DMSA-CdTe: 2,3-dimercapto-succinic acid-stabilized CdTe; ITO: indium tin oxide; LTBI: latent tuberculosis infections; MG: malachite green; μ -PADs: microfluidic paper-based analytical devices; FCA: ferrocene-carboxylic acid; MIP: molecularly imprinted platform; nGO@TiO₂NLPs: nanoluminophore nanographene oxide wrapping titanium dioxide; PAMAM-CIZS/ZnS QDs: PAMAM-CuInZnS/ZnS quantum dots; NSs: nanosheets; CO: 7-(diethylamino) coumarin-3-carboxylic acid; NA: 3-(4-amino-1,8-naphthalimid) propanoic acid; OLEDs: organic light-emitting diodes; SECLDs: solid-state electrochemiluminescence devices; CS-AgI: chitosan-functionalized silver iodide; JPs: Janus particles; DA: Dopamine; AFB1: Aflatoxin B1; CT: calcitonin; CS-AgI: chitosan functionalized silver iodide; PNK: polynucleotide kinase; Con A: concanavalin A; HE4: human epididymis protein 4; SA: Sialic acid; cTnI: cardiac troponin I; EP: ethyl paraoxon; PKA: protein kinase A; c-PFBT NPs: carboxyl-functionalized poly((9,9-dioctylfluorenyl-2,7-diyl)-co-(1,4-benzo-thia-da-zole)) nanoparticles; L-CdS QDs: L-cysteine capped CdS quantum dots; OPs: organophosphorus pesticides; Hx: hypoxanthine; CA: chlorogenic acid; TB: thrombin.

Acknowledgements

This work was supported by the grants from the Natural Science Foundation of Chongqing (cstc2020jcyj-msxmX0330, cstc2021jcyj-yzysbA0057); the National Natural Science Foundation of China (31971242, 12032007); the Chongqing Science, the Technology Bureau (cstc2019jcyj-zdxmX0028, cstc2020jscx-msxmX0132); the Project of Tutorial System of Medical Undergraduate in Lab Teaching & Management Center in Chongqing Medical

University (LTMCMTS202005) and the JinFeng Laboratory Foundation, Chongqing, China (jfkjyf202203001).

Competing Interests

The authors have declared that no competing interest exists.

References

- Liu X, Zhao S, Tan L, Tan Y, Wang Y, Ye Z, et al. Frontier and hot topics in electrochemiluminescence sensing technology based on CiteSpace bibliometric analysis. *Biosens Bioelectron.* 2022; 201: 113932.
- Feng Y-G, Zhu J-H, Wang A-J, Mei L-P, Luo X, Feng J-J. AuPt nanocrystals/polydopamine supported on open-pored hollow carbon nanospheres for a dual-signaling electrochemical ratiometric immunosensor towards h-FABP detection. *Sens Actuators, B.* 2021; 346: 130501.
- Chen M, Ning Z, Chen K, Zhang Y, Shen Y. Recent advances of electrochemiluminescent system in bioassay. *J Anal Test.* 2020; 4: 57-75.
- Ning Z, Chen M, Wu G, Zhang Y, Shen Y. Recent advances of functional nucleic acids-based electrochemiluminescent sensing. *Biosens Bioelectron.* 2021; 191: 113462.
- Wang Y-Z, Hao N, Feng Q-M, Shi H-W, Xu J-J, Chen H-Y. A ratiometric electrochemiluminescence detection for cancer cells using g-C₃N₄ nanosheets and Ag-PAMAM-luminol nanocomposites. *Biosens Bioelectron.* 2016; 77: 76-82.
- Zhao S, Zang G, Zhang Y, Liu H, Wang N, Cai S, et al. Recent advances of electrochemical sensors for detecting and monitoring ROS/RNS. *Biosens Bioelectron.* 2021; 179: 113052.
- Xia H, Li L, Yin Z, Hou X, Zhu J-J. Biobar-coded gold nanoparticles and DNAzyme-based dual signal amplification strategy for ultrasensitive detection of protein by electrochemiluminescence. *ACS Appl Mater Interfaces.* 2015; 7: 696-703.
- Du FX, Chen YQ, Meng CD, Lou BH, Zhang W, Xu GB. Recent advances in electrochemiluminescence immunoassay based on multiple-signal strategy. *Curr Opin Electrochem.* 2021; 28.
- Qiu J, Xu J, Zhang K, Gu W, Nie L, Wang G, et al. Refining cancer management using integrated liquid biopsy. *Theranostics.* 2020; 10: 2374.
- Su L, Shu T, Wang Z, Cheng J, Xue F, Li C, et al. Immobilization of bovine serum albumin-protected gold nanoclusters by using polyelectrolytes of opposite charges for the development of the reusable fluorescent Cu²⁺-sensor. *Biosens Bioelectron.* 2013; 44: 16-20.
- Wang Y, Luo J, Liu J, Sun S, Xiong Y, Ma Y, et al. Label-free microfluidic paper-based electrochemical aptasensor for ultrasensitive and simultaneous multiplexed detection of cancer biomarkers. *Biosens Bioelectron.* 2019; 136: 84-90.
- Deng S, Ju H. Electrogenated chemiluminescence of nanomaterials for bioanalysis. *Analyst.* 2013; 138: 43-61.
- Huo X-L, Lu H-J, Xu J-J, Zhou H, Chen H-Y. Recent advances of ratiometric electrochemiluminescence biosensors. *J Mater Chem B.* 2019; 7: 6469-75.
- Doeven EH, Barbante GJ, Hogan CF, Francis PS. Potential-resolved electrogenerated chemiluminescence for the selective detection of multiple luminophores. *ChemPlusChem.* 2015; 80: 456-70.
- Yang Z, Zong C, Yan F, Ju H. Automated chemiluminescent dual-analyte immunoassay based on resolved immunosensing channels. *Talanta.* 2010; 82: 1462-7.
- Li Z, Wu S, Zou G. Highly potential-resolved anodic electrochemiluminescence multiplexing immunoassay with CuInS₂@ZnS nanocrystals and [Ru(bpy)₂(dcbpy)]²⁺ as emitters. *J Electroanal Chem.* 2021; 888: 115173.
- Wang L, Gao G, Zhou Y, Xu T, Chen J, Wang R, et al. Tough, adhesive, self-Healable, and transparent ionically conductive zwitterionic nanocomposite hydrogels as skin strain sensors. *ACS Appl Mater Interfaces.* 2019; 11: 3506-15.
- Liu Z, Qi W, Xu G. Recent advances in electrochemiluminescence. *Chem Soc Rev.* 2015; 44: 3117-42.
- Zhu L, Yu L, Ye J, Yan M, Peng Y, Huang J, et al. A ratiometric electrochemiluminescence strategy based on two-dimensional nanomaterial-nucleic acid interactions for biosensing and logic gates operation. *Biosens Bioelectron.* 2021; 178: 113022.
- Li C, Fu Z, Li Z, Wang Z, Wei W. Cross-talk-free multiplexed immunoassay using a disposable electrochemiluminescent immunosensor array coupled with a non-array detector. *Biosens Bioelectron.* 2011; 27: 141-7.
- Ma C, Cao Y, Gou X, et al. Recent progress in electrochemiluminescence sensing and imaging. *Anal Chem.* 2019; 92: 431-454.
- Lv W, Ye H, Yuan Z, Liu X, Chen X, Yang W. Recent advances in electrochemiluminescence-based simultaneous detection of multiple targets. *Trends Analyt Chem.* 2020; 123: 115767.
- Shao K, Wang B, Ye S, Zuo Y, Wu L, Li Q, et al. Signal-amplified near-infrared ratiometric electrochemiluminescence aptasensor based on multiple quenching and enhancement effect of graphene/gold nanorods/G-quadruplex. *Anal Chem.* 2016; 88: 8179-87.

24. Liang R-P, Qiu W-B, Zhao H-F, Xiang C-Y, Qiu J-D. Electrochemiluminescence resonance energy transfer between graphene quantum dots and graphene oxide for sensitive protein kinase activity and inhibitor sensing. *Anal Chim Acta*. 2016; 904: 58-64.
25. Bertonecello P, Ugo P. Recent advances in electrochemiluminescence with quantum dots and arrays of nanoelectrodes. *ChemElectroChem*. 2017; 4: 1663-76.
26. Liu G, Jin B-K, Ma C, Chen Z, Zhu J-J. Potential-resolved electrochemiluminescence nanoprobes for visual apoptosis evaluation at single-cell level. *Anal Chem*. 2019; 91: 6363-70.
27. Li Z, Wu S, Zou G. Highly potential-resolved anodic electrochemiluminescence multiplexing immunoassay with CuInS₂@ ZnS nanocrystals and [Ru (bpy) ₂ (dcbpy)] ²⁺ as emitters. *J Electroanal Chem*. 2021; 888: 115173.
28. Hong C, Zhang X, Ye S, Yang H, Huang Z, Yang D, et al. Aptamer-pendant DNA tetrahedron nanostructure probe for ultrasensitive detection of tetracycline by coupling target-triggered rolling circle amplification. *ACS Appl Mater Interfaces*. 2021; 13: 19695-700.
29. Cao S-P, Luo Q-X, Li Y-J, Liang R-P, Qiu J-D. Gold nanoparticles decorated carbon nitride nanosheets as a coreactant regulate the conversion of the dual-potential electrochemiluminescence of Ru(bpy)₃²⁺ for Hg²⁺ detection. *Chem Commun*. 2020; 56: 5625-8.
30. Cheng Y, Huang Y, Lei J, Zhang L, Ju H. Design and biosensing of Mg²⁺-dependent DNzyme-triggered ratiometric electrochemiluminescence. *Anal Chem*. 2014; 86: 5158-63.
31. Zhang Y, Xu J, Zhou S, Zhu L, Lv X, Zhang J, et al. DNzyme-triggered visual and ratiometric electrochemiluminescence dual-readout assay for Pb(II) based on an assembled paper device. *Anal Chem*. 2020; 92: 3874-81.
32. Fang D, Zhang S, Dai H, Lin Y. An ultrasensitive ratiometric electrochemiluminescence immunosensor combining photothermal amplification for ovarian cancer marker detection. *Biosens Bioelectron*. 2019; 146: 111768.
33. Huang Y, Lei J, Cheng Y, Ju H. Ratiometric electrochemiluminescent strategy regulated by electrocatalysis of palladium nanocluster for immunosensing. *Biosens Bioelectron*. 2016; 77: 733-9.
34. Shao K, Wang B, Nie A, Ye S, Ma J, Li Z, et al. Target-triggered signal-on ratiometric electrochemiluminescence sensing of PSA based on MOF/Au/G-quadruplex. *Biosens Bioelectron*. 2018; 118: 160-6.
35. Fu X, Tan X, Yuan R, Chen S. A dual-potential electrochemiluminescence ratiometric sensor for sensitive detection of dopamine based on graphene-CdTe quantum dots and self-enhanced Ru(II) complex. *Biosens Bioelectron*. 2017; 90: 61-8.
36. Zhang H-R, Xu J-J, Chen H-Y. Electrochemiluminescence ratiometry: a new approach to DNA biosensing. *Anal Chem*. 2013; 85: 5321-5.
37. Zhu L, Zhang M, Ye J, Yan M, Zhu Q, Huang J, et al. Ratiometric electrochemiluminescence/electrochemical strategy for sensitive detection of microRNA based on duplex-specific nuclease and multilayer circuit of catalytic hairpin assembly. *Anal Chem*. 2020; 92: 8614-22.
38. Hu Y, Chen C, Liu Y, Wang S, Guo Z, Hu Y. Dual-signals electrochemiluminescence ratiometry based the synergic effect between luminol and CdSe quantum dots for direct detection of hydrogen peroxide. *J Electroanal Chem*. 2018; 815: 61-7.
39. Wu L, Ding F, Yin W, Ma J, Wang B, Nie A, et al. From electrochemistry to electroluminescence: development and application in a ratiometric aptasensor for aflatoxin B₁. *Anal Chem*. 2017; 89: 7578-85.
40. Cao Y, Zhu W, Wei H, Ma C, Lin Y, Zhu J-J. Stable and monochromatic all-Inorganic halide perovskite assisted by hollow carbon nitride nanosphere for ratiometric electrochemiluminescence bioanalysis. *Anal Chem*. 2020; 92: 4123-30.
41. Feng Y, Sun F, Chen L, Lei J, Ju H. Ratiometric electrochemiluminescence detection of circulating tumor cells and cell-surface glycans. *J Electroanal Chem*. 2016; 781: 48-55.
42. Ma C, Cao Y, Gou X, Zhu J-J. Recent progress in electrochemiluminescence sensing and imaging. *Anal Chem*. 2020; 92: 431-54.
43. Han T, Ma C, Wang L, Cao Y, Chen H-Y, Zhu J-J. A novel electrochemiluminescence janus emitter for dual-mode biosensing. *Adv Funct Mater*. 2022; 2200863.
44. Li J, Luo M, Yang H, Ma C, Cai R, Tan W. Novel dual-signal electrochemiluminescence aptasensor involving the resonance energy transfer system for kanamycin detection. *Anal Chem*. 2022; 94: 6410-6.
45. Lu Y, Ke H, Wang Y, Zhang Y, Li H, Huang C, et al. A ratiometric electrochemiluminescence resonance energy transfer platform based on novel dye BODIPY derivatives for sensitive detection of lactoferrin. *Biosens Bioelectron*. 2020; 170: 112664.
46. Wang Y, Shan D, Wu G, Wang H, Ru F, Zhang X, et al. A novel "dual-potential" ratiometric electrochemiluminescence DNA sensor based on enhancing and quenching effect by G-quadruplex / hemin and Au-Luminol bifunctional nanoparticles. *Biosens Bioelectron*. 2018; 106: 64-70.
47. Hao Q, Wang L, Niu S, Ding C, Luo X. Ratiometric electrogenerated chemiluminescence sensor based on a designed anti-fouling peptide for the detection of carcinoembryonic antigen. *Anal Chim Acta*. 2020; 1136: 134-40.
48. Cao J-T, Wang Y-L, Wang J-B, Zhou Q-M, Ma S-H, Liu Y-M. An electrochemiluminescence ratiometric self-calibrated biosensor for carcinoembryonic antigen detection. *J Electroanal Chem*. 2018; 814: 111-7.
49. Zhang G, Li M, Yu K, Chai H, Xu S, Xu T, et al. Two-dimensional metalloporphyrinic framework nanosheet-based dual-mechanism-driven ratiometric electrochemiluminescent biosensing of protein kinase activity. *ACS Appl Bio Mater*. 2021; 4: 1616-23.
50. Li J, Luo M, Jin C, Zhang P, Yang H, Cai R, et al. Plasmon-enhanced electrochemiluminescence of PTP-decorated Eu MOF-based Pt-tipped Au bimetallic nanorods for the lincomycin assay. *ACS Appl Mater Interfaces*. 2022; 14: 383-9.
51. Isildak I, Navaeipour F, Afsharan H, Kanberoglu GS, Agir I, Ozer T, et al. Electrochemiluminescence methods using CdS quantum dots in aptamer-based thrombin biosensors: a comparative study. *Mikrochim Acta*. 2020; 187: 1-13.
52. Isildak I, Navaeipour F, Afsharan H, Kanberoglu GS, Agir I, Ozer T, et al. Electrochemiluminescence methods using CdS quantum dots in aptamer-based thrombin biosensors: a comparative study. *Mikrochim Acta*. 2019; 187: 25.
53. Chen L, Wang X, Zhang Q, Li Z, Kang Q, Shen D. A ratiometric electrochemiluminescence method using a single luminophore of porous gC₃N₄ for the ultrasensitive determination of alpha fetoprotein. *Analyst*. 2020; 145: 2389-97.
54. Wang L, Xing B, Wang H, Hu L, Kuang X, Liang H, et al. Electrochemiluminescence immunosensor based on the quenching effect of CuO@ GO on m-CNNS for cTnI detection. *Anal Biochem*. 2021; 612: 114012.
55. Fu XM, Tan XR, Yuan R, Chen SH. A dual-potential electrochemiluminescence ratiometric sensor for sensitive detection of dopamine based on graphene-CdTe quantum dots and self-enhanced Ru(II) complex. *Biosens Bioelectron*. 2017; 90: 61-8.
56. Zheng H, Ke Y, Yi H, Dai H, Fang D, Lin Y, et al. A bifunctional reagent regulated ratiometric electrochemiluminescence biosensor constructed on surfactant-assisted synthesis of TiO₂ mesocrystals for the sensing of deoxyribovalenol. *Talanta*. 2019; 196: 600-7.
57. Yi K, Zi-Hui Z, Ping H, Ye-Lin L, Bao-Hua Z, Li-Juan C, et al. Multiple modes of electrochemiluminescence using thermally activated delayed fluorescent polymer. *Chinese J Anal Chem*. 2021; 49: 1015-24.
58. Lei Y-M, Huang W-X, Zhao M, Chai Y-Q, Yuan R, Zhuo Y. Electrochemiluminescence resonance energy transfer system: mechanism and application in ratiometric aptasensor for lead ion. *Anal Chem*. 2015; 87: 7787-94.
59. Zhang Y, Xu J, Zhou S, Zhu L, Lv X, Zhang J, et al. DNzyme-triggered visual and ratiometric electrochemiluminescence dual-readout assay for Pb(II) based on an assembled paper device. *Anal Chem*. 2020; 92: 3874-81.
60. Guo Z, Qiao B, Guo Q, Zhang H, Cai C, Feng J-J. Dual-signal ratiometric electrochemiluminescence assay for detecting the activity of human methyltransferase. *Analyst*. 2018; 143: 3353-9.
61. Zhang C, Liu D, Zhang H, Tan X, Chen S. A ratiometric electrochemiluminescent immunoassay for calcitonin by using N-(aminobutyl)-N-(ethylisoluminol) and graphite-like carbon nitride. *Mikrochim Acta*. 2019; 186: 1-9.
62. Fang DD, Zeng BS, Zhang SP, Dai H, Lin YY. A self-enhanced electrochemiluminescent ratiometric zearalenone immunoassay based on the use of helical carbon nanotubes. *Mikrochim Acta*. 2020; 187: 1-9.
63. Fang D, Zeng B, Zhang S, Dai H, Lin Y. A self-enhanced electrochemiluminescent ratiometric zearalenone immunoassay based on the use of helical carbon nanotubes. *Mikrochim Acta*. 2020; 187: 1-9.
64. Feng Y, Shi L, Wu H, Chen L, Chi Y. Detection of cyanide by etching-induced electrochemiluminescence recovery. *Electrochim Acta*. 2018; 261: 29-34.
65. Zhang G, Chai H, Tian M, Zhu S, Qu L, Zhang X. Zirconium-metalloporphyrin frameworks-luminol competitive electrochemiluminescence for ratiometric detection of polynucleotide kinase activity. *Anal Chem*. 2020; 92: 7354-62.
66. Zhang H, Zhang C, Liu D, Zuo F, Chen S, Yuan R, et al. A ratiometric electrochemiluminescent biosensor for Con A detecting based on competition of dissolved oxygen. *Biosens Bioelectron*. 2018; 120: 40-6.
67. Wang J, Song J, Zheng H, Zheng X, Dai H, Hong Z, et al. Application of NiFe₂O₄ nanotubes as catalytically promoted sensing platform for ratiometric electrochemiluminescence analysis of ovarian cancer marker. *Sens Actuators, B*. 2019; 288: 80-7.
68. Cao N, Zhao F, Zeng B. A novel ratiometric molecularly imprinted electrochemiluminescence sensor for sensitive and selective detection of salicylic acid based on PEI-CdS quantum dots as anodic coreactant and cathodic luminophore. *Sens Actuators, B*. 2020; 313: 128042.
69. Han Z, Shu J, Liang X, Cui H. Label-Free Ratiometric electrochemiluminescence aptasensor based on nanographene oxide wrapped titanium dioxide nanoparticles with potential-resolved electrochemiluminescence. *Anal Chem*. 2019; 91: 12260-7.
70. Wang L, Liu P, Liu Z, Cao H, Ye S, Zhao K, et al. A dual-potential ratiometric electrochemiluminescence biosensor based on Au@ CDs nanoflowers, Au@ luminol nanoparticles and an enzyme-free DNA nanomachine for ultrasensitive p53 DNA detection. *Sens Actuators, B*. 2021; 327: 128890.
71. Zhang Q, Dai H, Wang T, Li Y, Zhang S, Xu G, et al. Ratiometric electrochemiluminescent immunoassay for tumor marker regulated by mesocrystals and biomimetic catalyst. *Electrochim Acta*. 2016; 196: 565-71.
72. Fan G-C, Ren X-L, Zhu C, Zhang J-R, Zhu J-J. A new signal amplification strategy of photoelectrochemical immunoassay for highly sensitive interleukin-6 detection based on TiO₂/CdS/CdSe dual co-sensitized structure. *Biosens Bioelectron*. 2014; 59: 45-53.

73. Yang G, He Y, Zhao J, Chen S, Yuan R. Ratiometric electrochemiluminescence biosensor based on Ir nanorods and CdS quantum dots for the detection of organophosphorus pesticides. *Sens Actuators, B*. 2021; 341: 130008.
74. Liu D, Yang G, Zhang X, Chen S, Yuan R. A novel potential-regulated ratiometric electrochemiluminescence sensing strategy based on poly(9,9-di-n-octylfluorenyl-2,7-diyl) polymer nanoparticles for microRNA detection. *Sens Actuators, B*. 2021; 329: 129210.
75. Chen H, Zhang H, Yuan R, Chen S. Novel double-potential electrochemiluminescence ratiometric strategy in enzyme-based inhibition biosensing for sensitive detection of organophosphorus pesticides. *Anal Chem*. 2017; 89: 2823-9.
76. Zuo F, Zhang H, Xie J, Chen S, Yuan R. A sensitive ratiometric electrochemiluminescence biosensor for hypoxanthine detection by *in situ* generation and consumption of coreactants. *Electrochim Acta*. 2018; 271: 173-9.
77. Wang Y, Gao C, Ge S, Zhang L, Yu J, Yan M. Self-powered sensing platform equipped with Prussian blue electrochromic display driven by photoelectrochemical cell. *Biosens Bioelectron*. 2017; 89: 728-34.
78. Zhang X, Ding S-N. Graphite paper-based bipolar electrode electrochemiluminescence sensing platform. *Biosens Bioelectron*. 2017; 94: 47-55.
79. Zhao W, Ma Y, Ye J, Jin J. A closed bipolar electrochemiluminescence sensing platform based on quantum dots: A practical solution for biochemical analysis and detection. *Sens Actuators, B*. 2020; 311: 127930.
80. Zhang Y-W, Cao Y, Mao C-J, Jiang D, Zhu W. An iron(III)-based metal-organic gel-catalyzed dual electrochemiluminescence system for cytosensing and *in situ* evaluation of the VEGF165 subtype. *Anal Chem*. 2022; 94: 4095-102.
81. He Y, Hu F, Zhao J, Yang G, Zhang Y, Chen S, et al. Bifunctional moderator-powered ratiometric electrochemiluminescence enzymatic biosensors for detecting organophosphorus pesticides based on dual-signal combined nanopores. *Anal Chem*. 2021; 93: 8783-90.
82. Liu D, Yang G, Zhang X, Chen S, Yuan R. A novel potential-regulated ratiometric electrochemiluminescence sensing strategy based on poly(9,9-di-n-octylfluorenyl-2,7-diyl) polymer nanoparticles for microRNA detection. *Sens Actuators, B*. 2021; 329: 129210.
83. Zhao J, He Y, Tan K, Yang J, Chen S, Yuan R. Novel ratiometric electrochemiluminescence biosensor based on BP-CdTe QDs with dual emission for detecting microRNA-126. *Anal Chem*. 2021; 93: 12400-8.
84. Cao S-P, Luo Q-X, Li Y-J, Liang R-P, Qiu J-D. Gold nanoparticles decorated carbon nitride nanosheets as a coreactant regulate the conversion of the dual-potential electrochemiluminescence of Ru (bpy) 3 2+ for Hg 2+ detection. *Chem Commun*. 2020; 56: 5625-8.
85. Chen H, Li W, Wang Q, Jin X, Nie Z, Yao S. Nitrogen doped graphene quantum dots based single-luminophore generated dual-potential electrochemiluminescence system for ratiometric sensing of Co2+ ion. *Electrochim Acta*. 2016; 214: 94-102.
86. Shang Q, Zhou Z, Shen Y, Zhang Y, Li Y, Liu S, et al. Potential-modulated electrochemiluminescence of carbon nitride nanosheets for dual-signal sensing of metal ions. *ACS Appl Mater Interfaces*. 2015; 7: 23672-8.
87. Hu Y, Su L, Wang S, Guo Z, Hu Y, Xie H. A ratiometric electrochemiluminescent tetracycline assay based on the combined use of carbon nanodots, Ru (bpy) 32+, and magnetic solid phase microextraction. *Mikrochim Acta*. 2019; 186: 1-10.
88. Wang Y-L, Liu F-R, Cao J-T, Ren S-W, Liu Y-M. Spatial-resolved dual-signal-output electrochemiluminescent ratiometric strategy for accurate and sensitive immunoassay. *Biosens Bioelectron*. 2018; 102: 525-30.
89. Feng X, Gan N, Lin S, Li T, Cao Y, Hu F, et al. Ratiometric electrochemiluminescent aptasensor array for antibiotic based on internal standard method and spatial-resolved technique. *Sens Actuators, B*. 2016; 226: 305-11.
90. Cao J-T, Fu X-L, Liu F-R, Ren S-W, Liu Y-M. Reduced graphene oxide-gold nanoparticles-catalase-based dual signal amplification strategy in a spatial-resolved ratiometric electrochemiluminescence immunoassay. *Analyst*. 2020; 145: 91-6.
91. Xu Y, Wang Z, Ding C, Luo X. Ratiometric antifouling electrochemiluminescence biosensor based on bi-functional peptides and low toxic quantum dots. *Sens Actuators, B*. 2020; 322.
92. Ding C, Li Y, Wang L, Luo X. Ratiometric electrogenerated chemiluminescence cytosensor based on conducting polymer hydrogel loaded with internal standard molecules. *Anal Chem*. 2019; 91: 983-9.
93. Xu Y, Wang Z, Ding C, Luo X. Ratiometric antifouling electrochemiluminescence biosensor based on bi-functional peptides and low toxic quantum dots. *Sens Actuators, B*. 2020; 322: 128613.
94. Ding C, Li Y, Wang L, Luo X. Ratiometric electrogenerated chemiluminescence cytosensor based on conducting polymer hydrogel loaded with internal standard molecules. *Anal Chem*. 2018; 91: 983-9.
95. Munge BS, Stracensky T, Gamez K, DiBiase D, Rusling JF. Multiplex immunosensor arrays for electrochemical detection of cancer biomarker proteins. *Electroanalysis*. 2016; 28: 2644-58.
96. Pakchin PS, Nakhjavani SA, Saber R, Ghanbari H, Omid Y. Recent advances in simultaneous electrochemical multi-analyte sensing platforms. *Trends Anal Chem*. 2017; 92: 32-41.
97. Chang J, Wang X, Wang J, Li H, Li F. Nucleic acid-functionalized metal-organic framework-based homogeneous electrochemical biosensor for simultaneous detection of multiple tumor biomarkers. *Anal Chem*. 2019; 91: 3604-10.
98. Tian J, Zhou L, Zhao Y, Wang Y, Peng Y, Zhao S. Multiplexed detection of tumor markers with multicolor quantum dots based on fluorescence polarization immunoassay. *Talanta*. 2012; 92: 72-7.
99. Zhao J, Du J, Luo J, Chen S, Yuan R. A novel potential-resolved electrochemiluminescence immunosensor for the simultaneous determination of brain natriuretic peptide and cardiac troponin I. *Sens Actuators, B*. 2020; 311: 127934.
100. Shao H, Lin H, Lu J, Hu Y, Wang S, Huang Y, et al. Potential-resolved Faraday cage-type electrochemiluminescence biosensor for simultaneous determination of miRNAs using functionalized g-C3N4 and metal organic framework nanosheets. *Biosens Bioelectron*. 2018; 118: 247-52.
101. Liu H, Liu Z, Yi J, Ma D, Xia F, Tian D, et al. A dual-signal electroluminescence aptasensor based on hollow Cu/Co-MOF-luminol and g-C3N4 for simultaneous detection of acetaminiprid and malathion. *Sens Actuators B-Chem*. 2021; 331: 129412.
102. He Y, Li J, Liu Y. Reusable and dual-potential responses electrogenerated chemiluminescence biosensor for synchronously cytosensing and dynamic cell surface N-glycan evaluation. *Anal Chem*. 2015; 87: 9777-85.
103. Valentini G, Bruno C, Rapino S, Fiorani A, Jackson EA, Scott LT, et al. Intense and tunable electrochemiluminescence of corannulene. *J Phys Chem C*. 2010; 114: 19467-72.
104. Cheng L, Liu X, Lei J, Ju H. Low-potential electrochemiluminescent sensing based on surface unpassivation of CdTe quantum dots and competition of analyte cation to stabilizer. *Anal Chem*. 2010; 82: 3359-64.
105. Ji J, Wen J, Shen Y, Lv Y, Chen Y, Liu S, et al. Simultaneous noncovalent modification and exfoliation of 2D carbon nitride for enhanced electrochemiluminescent biosensing. *J Am Chem Soc*. 2017; 139: 11698-701.
106. Kitta SA, Gao W, Zhulodov YT, Qi L, Nsabimana A, Liu Z, et al. Stainless steel electrode for sensitive luminol electrochemiluminescent detection of H2O2, glucose, and glucose oxidase activity. *Anal Chem*. 2017; 89: 9864-9.
107. Kovalchuk EP, Reshetnyak OV, Chernyak AO, Kovalyshyn YS. Electrochemiluminescence on np1-metals: I. the analysis of chemiluminescent reactions. *Electrochim Acta*. 1999; 44: 4079-86.
108. Lei Y-M, Zhou J, Chai Y-Q, Zhuo Y, Yuan R. SnS2 quantum dots as new emitters with strong electrochemiluminescence for ultrasensitive antibody detection. *Anal Chem*. 2018; 90: 12270-7.
109. Liu Y, Chen X, Wang M, Ma Q. A visual electrochemiluminescence resonance energy transfer/surface plasmon coupled electrochemiluminescence nanosensor for Shiga toxin-producing Escherichia coli detection. *Green Chem*. 2018; 20: 5520-7.
110. Xu L-L, Zhang W, Shang L, Ma R-n, Jia L-p, Jia W-l, et al. Perylenetetracarboxylic acid and carbon quantum dots assembled synergistic electrochemiluminescence nanomaterial for ultra-sensitive carcinoembryonic antigen detection. *Biosens Bioelectron*. 2018; 103: 6-11.
111. Lee SK, Zu Y, Herrmann A, Geerts Y, Müllen K, Bard AJ, et al. Electrochemistry, spectroscopy and electrogenerated chemiluminescence of perylene, terylene, and quaterylene diimides in aprotic solution. *J Am Chem Soc*. 1999; 121: 3513-20.
112. Williams ME, Murray RW. Perylene polyether hybrids: Highly soluble, luminescent, redox-active dyes. *Chem Mater*. 1998; 10: 3603-10.
113. Gao H, Dang Q, Xia S, Zhao Y, Qi H, Gao Q, et al. Highly selective electrogenerated chemiluminescence biosensor for simultaneous detection of matrix metalloproteinase-2 and matrix metalloproteinase-7 in cell secretions. *Sens Actuators B Chem*. 2017; 253: 69-76.
114. Song Y, Zhang W, He S, Shang L, Ma R, Jia L, et al. Perylene diimide and luminol as potential-resolved electrochemiluminescence nanoprobe for dual targets immunoassay at low potential. *ACS Appl Mater Interfaces*. 2019; 11: 33676-83.
115. Liu X, Jiang H, Fang Y, Zhao W, Wang N, Zang G, et al. Quantum dots based potential-resolution dual-targets electrochemiluminescence immunosensor for subtype of tumor marker and its serological evaluation. *Anal Chem*. 2015; 87: 9163-9.
116. Zhou B, Zhu M, Hao Y, Yang P. Potential-resolved electrochemiluminescence for simultaneous determination of triple latent tuberculosis infection markers. *ACS Appl Mater Interfaces*. 2017; 9: 30536-42.
117. Feng X, Gan N, Zhang H, Yan Q, Li T, Cao Y, et al. A novel dual-potential electrochemiluminescence aptasensor array using CdS quantum dots and luminol-gold nanoparticles as labels for simultaneous detection of malachite green and chloramphenicol. *Biosens Bioelectron*. 2015; 74: 587-93.
118. Guo Z, Wu L, Hu Y, Wang S, Li X. Potential-resolved "in-electrode" type electrochemiluminescence immunoassay based on functionalized g-C3N4 nanosheet and Ru-NH2 for simultaneous determination of dual targets. *Biosens Bioelectron*. 2017; 95: 27-33.
119. Han F, Jiang H, Fang D, Jiang D. Potential-resolved electrochemiluminescence for determination of two antigens at the cell surface. *Anal Chem*. 2014; 86: 6896-902.
120. Su L, Jiang Z, Tian Z, Wang H, Wang H, Zi Y, et al. Self-powered, ultrasensitive, and high-resolution visualized flexible pressure sensor based on color-tunable triboelectrification-induced electroluminescence. *Nano Energy*. 2021; 79: 105431.
121. Su L, Wang H, Tian Z, Wang H, Cheng Q, Yu W, et al. Low detection limit and high sensitivity wind speed sensor based on triboelectrification-induced electroluminescence. *Adv Sci*. 2019; 6: 1901980.

122. Wang S, Ge L, Zhang Y, Song X, Li N, Ge S, et al. Battery-triggered microfluidic paper-based multiplex electrochemiluminescence immunodevice based on potential-resolution strategy. *Lab Chip*. 2012; 12: 4489-98.
123. Li S, Wang S, Yan M, Ge S, Ge L, Yu J, et al. Rechargeable battery-based constant-potential electrochemiluminescence multiplexed immunoassay on single working electrode for sequentially anodic and cathodic detection through a self-assembly toggle switch. *Sens Actuators B Chem*. 2013; 183: 488-95.
124. Zhang L, Ying Y, Li Y, Fu Y. Integration and synergy in protein-nanomaterial hybrids for biosensing: Strategies and in-field detection applications. *Biosens Bioelectron*. 2020; 154: 112036.
125. Dong Y-P, Zhou Y, Wang J, Zhu J-J. Electrogenerated chemiluminescence resonance energy transfer between Ru (bpy) 3²⁺ electrogenerated chemiluminescence and gold nanoparticles/graphene oxide nanocomposites with graphene oxide as coreactant and its sensing application. *Anal Chem*. 2016; 88: 5469-75.
126. Shi X, Yang F, Liu H, Zhang M, Sun X, Guo Y, et al. Supersensitive electrochemiluminescence aptasensor for malathion residues based on ATO@TiO₂ and AgNPs. *Food Anal Methods*. 2021; 14: 2288-97.
127. Zhu Q, Mao W, Zhang C, Zhou Y, Tang Z, Yu C, et al. Au@ BSA microspheres-luminol and a novel luminescent zeolitic imidazolate framework were used for potential-resolved electrochemiluminescence to detect dual targets. *Anal Chim Acta*. 2020; 1140: 89-98.
128. Martínez-Periñán E, Gutiérrez-Sánchez C, García-Mendiola T, Lorenzo E. Electrochemiluminescence biosensors using screen-printed electrodes. *Biosensors*. 2020; 10: 118.
129. Yang M, Chen L, Guo L, Qiu B, Lin Z. High sensitive electrochemiluminescence biosensor based on Ru (phen)₃²⁺ loaded double strand DNA as signal tags used to detect DNA methyltransferase activity. *Electroanalysis*. 2022; 34: 387-396.
130. Li Z, Wu S, Zhang B, Fu L, Zou G. Promising mercaptobenzoic acid-bridged charge transfer for electrochemiluminescence from CuInS₂@ ZnS nanocrystals via internal Cu⁺/Cu²⁺ couple cycling. *J Phys Chem Lett*. 2019; 10: 5408-13.
131. Cao J-T, Liu F-R, Fu X-L, Ma J-X, Ren S-W, Liu Y-M, et al. A novel electrochemiluminescence resonance energy transfer system for simultaneous determination of two acute myocardial infarction markers using versatile gold nanorods as energy acceptors. *Chem Commun*. 2019; 55: 2829-32.
132. Chai Y, Tian D, Cui H. Electrochemiluminescence biosensor for the assay of small molecule and protein based on bifunctional aptamer and chemiluminescent functionalized gold nanoparticles. *Anal Chim Acta*. 2012; 715: 86-92.
133. Zhuo Y, Wang H-J, Lei Y-M, Zhang P, Liu J-L, Chai Y-Q, et al. Electrochemiluminescence biosensing based on different modes of switching signals. *Analyst*. 2018; 143: 3230-48.
134. Guo W, Ding H, Gu C, Liu Y, Jiang X, Su B, et al. Potential-resolved multicolor electrochemiluminescence for multiplex immunoassay in a single sample. *J Am Chem Soc*. 2018; 140: 15904-15.
135. Bruce D, Richter MM. Green electrochemiluminescence from ortho-metalated tris(2-phenylpyridine)iridium(III). *Anal Chem*. 2002; 74: 1340-2.
136. Dennany L, Forster RJ, White B, Smyth M, Rusling JF. Direct electrochemiluminescence detection of oxidized DNA in ultrathin films containing [Os(bpy)₂(PVP)₁₀]²⁺. *J Am Chem Soc*. 2004; 126: 8835-41.
137. Zhou J, Nie L, Zhang B, Zou G. Spectrum-resolved triplex-color electrochemiluminescence Multiplexing immunoassay with highly-passivated nanocrystals as tags. *Anal Chem*. 2018; 90: 12361-5.
138. Liu S, Zhang X, Yu Y, Zou G. Bandgap engineered and high monochromatic electrochemiluminescence from dual-stabilizers-capped CdSe nanocrystals with practical application potential. *Biosens Bioelectron*. 2014; 55: 203-8.
139. Tan X, Zhang B, Zou G. Electrochemistry and electrochemiluminescence of organometal halide perovskite nanocrystals in aqueous medium. *J Am Chem Soc*. 2017; 139: 8772-6.
140. Muegge BD, Richter MM. Multicolored electrogenerated chemiluminescence from ortho-metalated Iridium(III) systems. *Anal Chem*. 2004; 76: 73-7.
141. Du D, Shu J, Guo M, Haghghatbin MA, Yang D, Bian Z, et al. Potential-resolved differential electrochemiluminescence immunosensor for cardiac troponin I based on MOF-5-wrapped CdS quantum dot nanoluminophores. *Anal Chem*. 2020; 92: 14113-21.
142. Guo M, Shu J, Du D, Haghghatbin MA, Yang D, Bian Z, et al. A label-free three potential ratiometric electrochemiluminescence immunosensor for cardiac troponin I based on N-(4-aminobutyl)-N-ethylisoluminol functionalized graphene quantum dots. *Sens Actuat B-Chem*. 2021; 334:129628.
143. Lv Y, Zhou Z, Shen Y, Zhou Q, Ji J, Liu S, et al. Coupled fluorometer-potentiostat system and metal-free monochromatic luminophores for high-resolution wavelength-resolved electrochemiluminescent multiplex bioassay. *ACS Sensors*. 2018; 3: 1362-7.
144. Shu J, Han Z, Zheng T, Du D, Zou G, Cui H, et al. Potential-resolved multicolor electrochemiluminescence of N-(4-Aminobutyl)-N-ethylisoluminol/tetra(4-carboxyphenyl)porphyrin/TiO₂ nanoluminophores. *Anal Chem*. 2017; 89: 12636-40.
145. Wang Y-Z, Ji S-Y, Xu H-Y, Zhao W, Xu J-J, Chen H-Y, et al. Bidirectional electrochemiluminescence color switch: an application in detecting multimarkers of prostate cancer. *Anal Chem*. 2018; 90: 3570-5.
146. Han F, Jiang H, Fang D, Jiang D. Potential-resolved electrochemiluminescence for determination of two antigens at the cell surface. *Anal Chem*. 2014; 86: 6896-902.
147. Soulsby LC, Doeven EH, Pham TT, Eyckens DJ, Henderson LC, Long BM, et al. Colour tuning and enhancement of gel-based electrochemiluminescence devices utilising Ru(II) and Ir(III) complexes. *Chem Commun*. 2019; 55: 11474-7.
148. Voci S, Duwald R, Grass S, Hayne DJ, Bouffier L, Francis PS, et al. Self-enhanced multicolor electrochemiluminescence by competitive electron-transfer processes. *Chem Sci*. 2020; 11: 4508-15.
149. Kim JI, Shin I-S, Kim H, Lee J-K. Efficient electrogenerated chemiluminescence from cyclometalated Iridium(III) complexes. *J Am Chem Soc*. 2005; 127: 1614-5.
150. Kiran RV, Hogan CF, James BD, Wilson DJD. Photophysical and electrochemical properties of phenanthroline-based bis-cyclometalated Iridium complexes in aqueous and organic media. *Eur J Inorg Chem* 2011; 2011: 4816-25.
151. Swanick KN, Ladouceur S, Zysman-Colman E, Ding Z. Self-enhanced electrochemiluminescence of an Iridium(III) complex: mechanistic insight. *Angew Chem Int Ed Engl*. 2012; 51: 11079-82.
152. Zanarini S, Felici M, Valenti G, Marccaccio M, Prodi L, Bonacchi S, et al. Green and blue electrochemically generated chemiluminescence from click chemistry-customizable Iridium complexes. *Chem Eur J*. 2011; 17: 4640-7.
153. Zanarini S, Rampazzo E, Bonacchi S, Juris R, Marccaccio M, Montalti M, et al. Iridium doped Silica-PEG nanoparticles: enabling electrochemiluminescence of neutral complexes in aqueous media. *J Am Chem Soc*. 2009; 131: 14208-9.
154. Gao FG, Bard AJ. Solid-state organic light-emitting diodes based on tris(2,2'-bipyridine)ruthenium(II) complexes. *J Am Chem Soc*. 2000; 122: 7426-7.
155. He L, Duan L, Qiao J, Wang R, Wei P, Wang L, et al. Blue-emitting cationic Iridium complexes with 2-(1H-Pyrazol-1-yl)pyridine as the ancillary ligand for efficient light-emitting electrochemical cells. *Adv Funct Mater*. 2008; 18: 2123-31.
156. Slinker JD, Gorodetsky AA, Lowry MS, Wang J, Parker S, Rohl R, et al. Efficient yellow electrochemiluminescence from a single layer of a cyclometalated Iridium complex. *J Am Chem Soc*. 2004; 126: 2763-7.
157. Su H-C, Chen H-F, Fang F-C, Liu C-C, Wu C-C, Wong K-T, et al. Solid-state white light-emitting electrochemical cells using Iridium-based cationic transition metal complexes. *J Am Chem Soc*. 2008; 130: 3413-9.
158. Wang F, Wang P, Fan X, Dang X, Zhen C, Zou D, et al. Voltage-controlled multicolor emitting devices. *Appl Phys Lett*. 2006; 89: 183519.
159. Welter S, Brunner K, Hofstraat JW, De Cola L. Electroluminescent device with reversible switching between red and green emission. *Nature*. 2003; 421: 54-7.
160. Doeven EH, Zammit EM, Barbante GJ, Francis PS, Barnett NW, Hogan CF, et al. A potential-controlled switch on/off mechanism for selective excitation in mixed electrochemiluminescent systems. *Chem Sci*. 2013; 4: 977-82.
161. Doeven EH, Zammit EM, Barbante GJ, Hogan CF, Barnett NW, Francis PS, et al. Selective excitation of concomitant electrochemiluminescence: tuning emission color by electrode potential. *Angew Chem Int Edit*. 2012; 51: 4354-7.
162. Guo Z, Hao T, Du S, Chen B, Wang Z, Li X, et al. Multiplex electrochemiluminescence immunoassay of two tumor markers using multicolor quantum dots as labels and graphene asconductingbridge. *Biosens Bioelectron*. 2013; 44: 101-7.
163. Muegge BD, Richter MM. Electrogenerated chemiluminescence from polymer-bound ortho-metalated iridium(III) systems. *Luminescence*. 2005; 20: 76-80.
164. Tokel NE, Bard AJ. Electrogenerated chemiluminescence. IX. Electrochemistry and emission from systems containing tris(2,2'-bipyridine)ruthenium(II) dichloride. *J Am Chem Soc*. 1972; 94: 2862-3.
165. Dongare P, Myron BDB, Wang L, Thompson DW, Meyer TJ. [Ru(bpy)₃]²⁺ revisited. Is it localized or delocalized? How does it decay? *Coord Chem Rev*. 2017; 345: 86-107.
166. Van Houten J, Watts RJ. Temperature dependence of the photophysical and photochemical properties of the tris(2,2'-bipyridyl)ruthenium(II) ion in aqueous solution. *J Am Chem Soc*. 1976; 98: 4853-8.
167. Liu J-L, Zhao M, Zhuo Y, Chai Y-Q, Yuan R. Highly efficient intramolecular electrochemiluminescence energy transfer for ultrasensitive bioanalysis of aflatoxin M1. *Chem Eur J*. 2017; 23: 1853-9.
168. Sun S, Yang Y, Liu F, Fan J, Peng X, Kehr J, et al. Intra- and intermolecular interaction ECL study of novel ruthenium tris-bipyridyl complexes with different amine reductants. *Dalton T*. 2009: 7969-74.
169. Zhen C, Chuai Y, Lao C, Huang L, Zou D, Lee DN, et al. Incorporation of electrochromic and electrochemiluminescence in one organic light-emitting device. *Appl Phys Lett*. 2005; 87: 093508.
170. Doeven EH, Zammit EM, Barbante GJ, Francis PS, Barnett NW, Hogan CF, et al. A potential-controlled switch on/off mechanism for selective excitation in mixed electrochemiluminescent systems. *Chem Sci*. 2013; 4: 977-82.
171. Schmittel M, Shu Q, Cinar ME. Tuning the wavelength of electrochemiluminescence by anodic potential: a design using non-Kekule-structured iridium-ruthenium luminophores. *Dalton Trans*. 2012; 41: 6064-8.
172. Doeven EH, Barbante GJ, Kerr E, Hogan CF, Ender JA, Francis PS, et al. Red-green-blue electrogenerated chemiluminescence utilizing a digital camera as detector. *Anal Chem*. 2014; 86: 2727-32.
173. Barbante GJ, Hogan CF, Wilson DJ, Lewcenko NA, Pfeffer FM, Barnett NW, et al. Simultaneous control of spectroscopic and photochemical properties in functionalised electrochemiluminescent tris(2,2'-bipyridine)ruthenium(II) complexes. *Analyst*. 2011; 136: 1329-38.
174. Barbante GJ, Doeven EH, Kerr E, Connell TU, Donnelly PS, White JM, et al. Understanding electrogenerated chemiluminescence efficiency in blue-shifted

- Iridium(III)-complexes: an experimental and theoretical study. *Chem Eur J*. 2014; 20: 3322-32.
175. Kerr E, Doeven EH, Barbante GJ, Hogan CF, Bower DJ, Donnelly PS, et al. Annihilation electrogenerated chemiluminescence of mixed metal chelates in solution: modulating emission colour by manipulating the energetics. *Chem Sci*. 2015; 6: 472-9.
176. Lv Q, Wang X D, Liao L S. Exploring axial organic multiblock heterostructure nanowires: advances in molecular design, synthesis, and functional applications. *Adv Funct Mater*. 2022; 2202364.
177. Moon HC, Lodge TP, Frisbie CD. Solution-processable electrochemiluminescent ion gels for flexible, low-voltage, emissive displays on plastic. *J Am Chem Soc*. 2014; 136: 3705-12.
178. D'Alton L, Nguyen P, Carrara S, et al. Intense near-infrared electrochemiluminescence facilitated by energy transfer in bimetallic Ir-Ru metallopolymer. *Electrochim Acta*. 2021; 379: 138117.
179. Sandroni M, Zysman-Colman E. Exploring energy transfer in luminescent heterometallic ruthenium-iridium ion pairs. *Dalton Trans*. 2014; 43: 3676-80.
180. Swanick KN, Sandroni M, Ding Z, Zysman-Colman E. Enhanced electrochemiluminescence from a stoichiometric ruthenium(II)-Iridium(III) complex soft salt. *Chem*. 2015; 21: 7435-40.
181. Green MLH, Hamnett A, Qin J, Baird P, Bandy JA, Prout K, et al. New organometallic solids: synthesis and solid state properties of salts of redoxactive organometallic clusters. *J Chem Soc Chem Commun*. 1987: 1811-4.
182. Kerr E, Doeven EH, Barbante GJ, Hogan CF, Hayne DJ, Donnelly PS, et al. New perspectives on the annihilation electrogenerated chemiluminescence of mixed metal complexes in solution. *Chem Sci*. 2016; 7: 5271-9.
183. Wang Y-Z, Xu C-H, Zhao W, Guan Q-Y, Chen H-Y, Xu J-J, et al. Bipolar electrode based multicolor electrochemiluminescence biosensor. *Anal Chem*. 2017; 89: 8050-6.
184. Soulsby LC, Hayne DJ, Doeven EH, Chen L, Hogan CF, Kerr E, et al. Electrochemically, spectrally, and spatially resolved annihilation-electrogenerated chemiluminescence of mixed-metal complexes at working and counter electrodes. *ChemElectroChem*. 2018; 5: 1543-7.
185. Holze R. Book Review: *Electrochemical Methods. Fundamentals and Applications* (2nd Edition). By Allen J. Bard and Larry R. Faulkner. *Angew Chem Int Ed*. 2002; 41: 655-7.
186. Luo Y, Lv F, Wang M, Lu L, Liu Y, Xiong X, et al. A multicolor electrochemiluminescence device based on closed bipolar electrode for rapid visual screening of *Salmonella typhimurium*. *Sensor Actuat B-Chem*. 2021; 349: 130761.
187. Wasalathanthri DP, Li D, Song D, Zheng Z, Choudhary D, Jansson I, et al. Elucidating organ-specific metabolic toxicity chemistry from electrochemiluminescent enzyme/DNA arrays and bioreactor bead-LC-MS/MS. *Chem Sci*. 2015; 6: 2457-68.
188. Hesari M, Swanick KN, Lu J-S, Whyte R, Wang S, Ding Z, et al. Highly efficient dual-color Electrochemiluminescence from BODIPY-capped PbS nanocrystals. *J Am Chem Soc*. 2015; 137: 11266-9.
189. Shu J, Han Z, Zheng T, Du D, Zou G, Cui H, et al. Potential-resolved multicolor electrochemiluminescence of N-(4-Aminobutyl)-N-ethylisoluminol/tetra(4-carboxyphenyl)porphyrin/TiO₂ nanoluminophores. *Anal Chem*. 2017; 89: 12636-40.
190. Ge L, Yan J, Song X, Yan M, Ge S, Yu J, et al. Three-dimensional paper-based electrochemiluminescence immunodevice for multiplexed measurement of biomarkers and point-of-care testing. *Biomaterials*. 2012; 33: 1024-31.
191. Qu L, Peng X. Control of photoluminescence properties of CdSe nanocrystals in growth. *J Am Chem Soc*. 2002; 124: 2049-55.
192. Sreejith S, Huong TTM, Borah P, Zhao Y. Organic-inorganic nanohybrids for fluorescence, photoacoustic and Raman bioimaging. *Sci Bull*. 2015; 60: 665-78.
193. Zhang J, Dong L, Yu S-H. A selective sensor for cyanide ion (CN⁻) based on the inner filter effect of metal nanoparticles with photoluminescent carbon dots as the fluorophore. *Sci Bull*. 2015; 60: 785-91.
194. Li Q-L, Ding S-N. Multicolor electrochemiluminescence of core-shell CdSe@ZnS quantum dots based on the size effect. *Sci China Chem*. 2016; 59: 1508-12.
195. Liu J-X, Ding S-N. Multicolor electrochemiluminescence of cadmium sulfide quantum dots to detect dopamine. *J Electroanal Chem*. 2016; 781: 395-400.
196. Bao L, Sun L, Zhang Z-L, Jiang P, Wise FW, Abruña HD, et al. Energy-level-related response of cathodic electrogenerated-chemiluminescence of self-assembled CdSe/ZnS quantum dot films. *J Phys Chem C*. 2011; 115: 18822-8.
197. Guo Z, Dong S, et al. Electrogenerated chemiluminescence determination of dopamine and epinephrine in the presence of ascorbic acid at carbon nanotube/nafion-Ru (bpy) 32+ composite film modified glassy carbon electrode. *Electroanalysis*. 2005; 17: 607-612.
198. Li B, Zhou Y, Wu W, Liu M, Mei S, Zhou Y, et al. Highly selective and sensitive determination of dopamine by the novel molecularly imprinted poly(nicotinamide)/CuO nanoparticles modified electrode. *Biosens Bioelectron*. 2015; 67: 121-8.
199. Samadi-maybodi A, Abbasi F, Akhoondi R. Aqueous synthesis and characterization of CdS quantum dots capped with some amino acids and investigations of their photocatalytic activities. *Colloid Surface A*. 2014; 447: 111-9.
200. Aboulaich A, Billaud D, Abyan M, Balan L, Gaumet J-J, Medjadhi G, et al. One-pot noninjection route to CdS Quantum Dots via hydrothermal synthesis. *ACS Appl Mater Interfaces*. 2012; 4: 2561-9.
201. Hua L, Han H, Zhang X. Size-dependent electrochemiluminescence behavior of water-soluble CdTe quantum dots and selective sensing of l-cysteine. *Talanta*. 2009; 77: 1654-9.
202. Yu WW, Qu L, Guo W, Peng X. Experimental determination of the extinction coefficient of CdTe, CdSe, and CdS nanocrystals. *Chem Mater*. 2003; 15: 2854-60.
203. Gao B-H, Ding S-N, Li Q-Q, Shan D, Sun Y-M, Cosnier S. Solid-state electrochemiluminescence of F-doped SnO₂ nanocrystals and its sensing application. *Electroanalysis*. 2012; 24: 1267-71.
204. Liu X, Jiang H, Lei J, Ju H. Anodic electrochemiluminescence of CdTe quantum dots and its energy transfer for detection of catechol derivatives. *Anal Chem*. 2007; 79: 8055-60.
205. Cao Z, Shu Y, Qin H, Su B, Peng X. Quantum dots with highly efficient, stable, and multicolor electrochemiluminescence. *ACS Cent Sci*. 2020; 6: 1129-37.